Journal of Medicinal Chemistry

Article

Synthesis and Evaluation of Diphenyl Conjugated Imidazole Derivatives as Potential Glutaminyl Cyclase Inhibitors for Treatment of Alzheimer's Disease

Manman Li, Yao Dong, Xi Yu, Yue Li, Yongdong Zou, Yizhi Zheng, Zhendan He, Zhigang Liu, Jun-Min Quan, Xianzhang Bu, and Haiqiang Wu

J. Med. Chem., **Just Accepted Manuscript** • DOI: 10.1021/acs.jmedchem.7b00648 • Publication Date (Web): 12 Jul 2017

ACS Publications

Journal of Medicinal Chemistry is published by the American Chemical Society. 1155 Sixteenth Street N.W., Washington, DC 20036

Synthesis and Evaluation of Diphenyl Conjugated Imidazole Derivatives as Potential Glutaminyl Cyclase Inhibitors for Treatment of Alzheimer's Disease

Manman Li,[§,#,¦] Yao Dong,[§,#,¦] Xi Yu,[§,#] Yue Li,[§] Yongdong Zou,[#] Yizhi Zheng,[#] Zhendan He,[§] Zhigang Liu,[¶] Junmin Quan,[†] Xianzhang Bu,[‡] Haiqiang Wu[§,#,φ,*]

[§] Department of Pharmacy, School of Medicine, Shenzhen University, Shenzhen, 518060, China

[#] College of Life Sciences and Oceanography, Shenzhen University, Shenzhen, 518060, China

[¶] School of Medicine, Shenzhen University, Shenzhen, 518060, China

[†] Key Laboratory of Structural Biology, School of Chemical Biology & Biotechnology, Peking University, Shenzhen Graduate School, Shenzhen 518055, China

[‡] School of Pharmaceutical Science, Sun Yat-sen University, Guangzhou, 510006, China

[φ] Department of Neurology, David Geffen School of Medicine, University of California, Los Angeles, CA, 90095, USA

[¦] Manman Li and Yao Dong contributed equally to this work.

Abstract:

High expression of glutaminyl cyclase (QC) contributes to the initiation of Alzheimer's disease (AD) by catalyzing the generation of neurotoxic pyroglutamate (pE)-modified β-amyloid (Aβ) peptides. Preventing the generation of pE-Aβs by QC inhibition has been suggested as a novel approach to a disease-modifying therapy for AD. In this work, a series of diphenyl conjugated imidazole derivatives (DPCIs) was rationally designed and synthesized. Analogues with this scaffold exhibited potent inhibitory activity against human QC (hQC), and good *in vitro* blood brain barrier (BBB) permeability. Further assessments corroborated that the selected hQC inhibitor **28** inhibits the activity of hQC and dramatically reduces the generation of pE-Aβs in cultured cells and *in vivo*, and improves the behavior of AD mice.

INTRODUCTION

Alzheimer's disease manifests as a progressive dementia that currently affects over 40 million people worldwide.[1] The devastating impact of AD on public health, the global economy, and society in general is widely recognized.[2] The hallmarks of AD are the presence of extracellular amyloid plaques composed of Aβ peptides (mainly $Aβ_{42}$ and $Aβ_{40}$) surrounded by activated glia and by intracellular neurofibrillary tangles composed of hyperphosphorylated tau protein, which makes Aβs and tau protein the prime drug targets for the development of anti-AD agents.[3]

The pathogenesis of AD has been extensively investigated, and the Aβ pathology, in which the Aβ peptides produced from proteolytic cleavage of the amyloid precursor protein (APP) by β- and γ-secretase, are believed to trigger AD pathogenesis via their aggregating forms, is well documented.[4, 5] In this regard, targeting Aβ pathology was considered a promising approach for prevention of AD and possibly other dementias. Unfortunately, though the behavior of AD can be improved in AD model mice by inhibiting the production, aggregation or increasing clearance of Aβ peptides, many key elements of the disease neurobiology remain controversial, and there is no reliable cure or disease-modifying therapy available for use before AD progresses to major memory loss and functional decline.[6] The consistent failure of drug candidates targeting late-stage Aβ pathology in clinical trials has led to a major shift towards exploring new causes involved in the very early phases of AD.[7, 8]

During the past decades a variety of N-truncated Aβs starting with amino residue ala-2, pyroglutamylated glu-3, phe-4, arg-5, pyroglutamylated glu-11, and so on, have been identified in AD brains.[7] Aβs undergo N-terminal truncation and cyclization of N-terminal glutamate (E) to pyroglutamate (pE), generating pE-$Aβ_{3-40/42}$ and pE-$Aβ_{11-40/42}$. These pE-Aβs, especially pE-$Aβ_{3-42}$, account for more than 50% of the total Aβ plaques in the AD brains.[9, 10] These modified Aβs have proteolytic resistance and increased hydrophobicity, they aggregate more rapidly than normal Aβs, seed further Aβ aggregation, and are more neurotoxic.[11-13] Importantly, pE-Aβs may be key initiators of AD pathogenesis in the early-stages of AD.[9, 10] Reducing the generation of pE-Aβs should promote more

efficient Aβ proteolysis and prevent aggregation by clearance of a major nucleation factor, and thus help prevent the initiation of the disease process.

The pyroglutamylation of N-truncated, N-ternimal glu-Aβs is catalyzed by glutaminyl cyclase (QC, also known as QPCT, EC 2.5.2.3)[13, 14] which is widely distributed in mammalian brain with robust expression in the hippocampus and cortex.[15, 16] Consistently increased expression of QC is correlated with the generation of pE-$A\beta_{3-42}$ and other Aβs in AD brains. Moreover, higher levels of QC mRNA are found in AD compared to age-matched normal brains, and a positive correlation between QC expression and the severity of AD has been confirmed.[17] It is revealed that QC inhibition attenuated the generation of pE-$A\beta_{3-4}$ in an AD model mouse brain and diminished the formation of Aβ plaques, and significantly improved the AD-like pathology.[18, 19] Thus, QC inhibitors may offer a new option for the development of novel anti-AD agents.[20] In view of this, a few QC inhibitors have been reported.[21-24] Typically, these inhibitors contain an aromatic motif tethered to an imidazole moiety, where the aromatic ring matches the hydrophobic space at the entrance of the active site, and the imidazole moiety is used to bind the catalytic zinc ion at the bottom of the pocket. For instance, the representative analogue **1** (PBD150, Figure 1A, upper), which was developed by Buchholz, et al.,[21] was found to be efficient in reducing the generation of pE-Aβ in a transgenic *Drosophila* model and also reduced AD pathology in several transgenic mouse models. Despite this proof of principle, however, these QC inhibitors have poor BBB permeability.[25] Therefore, the discovery of QC inhibitors with high activity and appropriate BBB penetrability is urgently needed to bring these novel anti-AD drugs to the clinic. Here, we describe the design and discovery of a series of DPCIs as potential QC inhibitors. These DPCIs retained the general properties required for reported inhibitory mechanisms but with enhanced inflexibility and BBB penetration, through conformational restriction and polarity tuning based on rational design. Our optimal DPCI shows higher QC inhibitory potency and improved *in vitro* BBB penetrability than **1**, and its beneficial effects on the pE-Aβ production and AD pathogenesis were validated in cell culture and in B6C3-Tg (APPswe/PSEN1dE9) double-transgenic mice.

RESULTS AND DISCUSSION

Design and synthesis of DPCIs

To search for efficient QC inhibitors, the interaction of reported analogue **1** with the human QC (hQC) was first based on the crystal structure of hQC in complex with **1** (PDB: 3PBB).[26] Of interest is the π-π stacking between the aromatic motif of **1** and phe325 at the hydrophobic entrance of the active site, the orthogonally-directed thiocarbamide starting linker, and the imidazole ring at the other terminal that runs deep into the narrow active site and binds with the catalytic zinc ion at the bottom of the pocket (Figure 1B and C). Therefore, it was predicted that flexibility of the thiocarbamide starting linker may limit the binding of **1** with QC; moreover, the presence of the thiocarbamide motif makes the linker hydrophilic, which would be expected to contribute to poor BBB penetrability. After these considerations, we replaced the thiocarbamide motif by an additional phenyl ring to generate a diphenyl moiety, and introduced an imidazole functionalized linker at the *ortho*-position of the new phenyl ring, to generate the new DPCI analogues. These modifications are anticipated to result in a more rigid conformation that will match the binding features by restricting the orthogonal conformation between the aromatic motif with the imidazole attached linker (Fig. 1B-C), and increase the hydrophobicity to favor BBB penetration. The basic structure of DPCIs is shown in Fig. 1A (bottom).

According to this concept, a series of DPCIs (**2-41**, Scheme 1) with various substitutions and different linker lengths were designed and synthesized (Scheme 1). Briefly, bromoaniline derivatives were coupled with phenylboronic acid derivatives to give the diphenyl intermediates **i** by Suzuki-Miyaura reactions under the catalysis of $Pd(DPPF)_2Cl_2$ and K_2CO_3, in 1,4-dioxane. Then the intermediates **i** reacted with 1,3-dibromopropane or 1,2-dibromoethane provided the intermediate **ii** in the presence of K_2CO_3 in acetonitrile. Finally, the nucleophile substitution reaction between **ii** and imidazole derivatives afforded the desired products in the presence of K_2CO_3 in acetonitrile.

Screening of DPCIs as hQC inhibitors

The hQC-glutamic acid dehydrogenase linked assay was used to evaluate the inhibitory potency of the

resulting compounds. The percentages of inhibition at 100 μM (% at 100 μM) toward hQC were recorded. As expected, compound **2** significantly inhibited the activity of hQC (85.34 %, Table 1). By modifying substitutions on ring A, we observed that the methyl substitution at R_3 (**3**), R_4 (**5**), or isopropyl substitution at R_5 (**6**) sharply decreased the inhibitory activity, while replacing the methyl at R_3 (**4**) with smaller F recovered the activity to an even higher level, indicating hinderance occurred by methyl substitution at the R_3, R_4, and R_5 positions. In contrast, the methyl substitution at R_6 (**7**) moderately increased the inhibitory potency (96.14 %), and F substitution at R_6 did not affect the activity as compared **10** with **8**. These observations are consistent with the predicted mode (Fig. 1B), wherein A ring presents at the entrance of the deep pocket, therefore the methyl substitution at inner positions R_3, R_4, or R_5 may limit the interaction of the compounds with hQC, while the R_6 points to the outside and allows substitutions with appropriate volume. In addition, replacing the 3',4'- dimethoxy at B ring with 3'- or 4'- F substitution apparently did not affect the binding as compared with the inhibitory activities of **2** with **8**, **11**, and **7** with **9,** respectively.

The 2nd batch of evaluation was focused on the analogues (**12-20**, Table 2) with a 2'-methyl substituted imidazole ring (C ring), and similar substitution patterns in rings A and B. These analogues generally showed low to moderate activities, and the 2'-methyl substitution at the C ring dramatically decreased the activity as compared to the inhibitory potency of **12**, **13**, **14**, **15**, **16**, **17** and **19** vs **3**, **5**, **6**, **8**, **9**, **10** and **11,** respectively. According to the proposed binding model, the zinc atom located at the bottle of the active site of hQC could be chelated by the 3'-N atom in the imidazole moiety. Therefore, it could be concluded that the decrease of their activities may be attributed to the blockage of the chelation by 2'-methyl substitution of the C ring.

Interestingly, unlike the 2'-methyl substitution, 4'-methyl substitution at the C ring moderately or slightly increased the activity as compared with the inhibition rate of **21**, **23**, **27**, **28**, **30**, **31** and **32** vs **2**, **4**, **7**, **8**, **9**, **10** and **11,** respectively (Table 3). More strikingly, compound **5**, which contains a methyl substitution in the R_4 position, was the least potent, nevertheless an additional introduction of methyl in

the 4'-position of imidazole motif led to compound **24** with sharply increased inhibitory potency (94.48 %). We reasoned that the 4'-methyl substitution at the imidazole ring may shift the binding site of **24** in hQC by the hydrophobic force between 4'-methyl and other residues in the native pocket. This would contribute to the chelation of the 3'-N atom in the imidazole motif with the zinc atom, and favor the direct interaction between the molecule and enzyme. In the presence of an R_3 methyl (**3**), or R_5 isopropyl (**6**), however, the 4'-methyl substitution in imidazole cannot achieve the optimal binding position as indicated by the dramatically decreased activity of **22** and **26,** respectively.

While designing the molecules, we noticed that a propyl linker is sufficient to deliver the imidazole motif to the zinc ion located at the bottom of the active site. To explore the effect of linker length on the inhibitory potency, analogues with a shorter ethyl linker instead of the propyl linker and similar substitution partners on rings A and C were further designed, synthesized and evaluated. All these compounds (**33-41**) showed poor potency on hQC inhibition as listed in Table 4, and the reduction of the linker length dramatically decreased the activity as compared to **33**, **35**, **36**, **37**, **38**, **39**, **40**, **41** with **2**, **21**, **8**, **15**, **28**, **11**, **19**, **32**, respectively. This observation indicated that the distance between the imidazole and biphenyl motif is critical to achieve favorable chelation of imidazole with the zinc ion on the bottom and the formation of π-π stacking of the aromatic motif with phe325 at the entrance of the hQC active site.

Based on the results mentioned above, the inhibitory IC_{50} values toward hQC of the analogues with percentages of inhibition > 80 % at 100 μM (**2**, **4**, **7**, **8**, **9**, **10**, **21**, **23**, **24**, **25**, **27**, **28**, **29**, **30**, **31**, **32**) were determined using **1** as a positive control. All compounds except **32** demonstrated a sub- or low micromolar IC_{50} (0.50-3.02 μM), which is lower than that of **1** (3.19 μM; Table 1 and 3). The structure-activity relationship (SAR) revealed by IC_{50} values is in accordance with rules indicated by the screening, wherein the 4'-methyl substitution at the imidazole motif generally increases the potency of hQC inhibition (**2**, **4**, **8**, **9** and **10** vs **21**, **23**, **28**, **30** and **31** respectively), and methyl substitutions closer to the linker are more harmful to the activity (**24**, **25**, **27**, **29** and **30**). Moreover, F substitution (**2** vs **4**,

21 vs **23**) at R_3, as well as F (**8** vs **10**, **28** vs **31**) or methyl (**2**, **8**, **21** and **28** vs **7**, **9**, **27** and **30,** respectively) substitution at R_6 increases activity to a variable extent.

To further understand the observed hQC inhibitory activity, molecular docking analysis of several potent inhibitors (**2**, **23**, and **28**) and the inactive inhibitors (**36** and **37**) was performed. The top ranked docked conformations for each compound were analyzed. The docked poses of the potent inhibitors (**2**, **23**, and **28**) resemble that of **1**. Both the π-π stacking between the terminal aromatic motif of the inhibitors and phe325 at the hydrophobic entrance of the active site, and the chelation between the imidazole ring and the catalytic zinc ion at the bottom of the pocket were conserved (Figure 2A-D). The binding of these potential DPCIs with hQC in the catalytic active region is predicted to be stronger. These compounds also exhibited increased potency of hQC inhibition compared with the positive control. In contrast, the poses of **36** and **37** deviate markedly from that of the potent inhibitors, the π-π stacking between the terminal aromatic motif of the inhibitors and phe325 of hQC is disrupted due to the shorter linker (Figure 2E and F). This also illuminated the SAR and hQC inhibitory potency of these designed DPCIs.

Compound 28 exhibits improved penetrability than 1 in PAMPA-BBB mode

One of the main concerns in the development of active chemicals targeting the central nervous system (CNS) is the BBB permeation. In the current work, the new derivatives were expected to have improved BBB permeability attributed to the introduction of the diphenyl moiety. This expectancy was supported by the prediction with ADMET-blood brain barrier descriptors using professional drug design software Discovery Studio. Two parameters, ADMET_BBB and ADMET_AlogP98, were used to evaluate the selected analogues and **1**, wherein ADMET_BBB means the base 10 logarithm of (brain concentration)/(blood concentration) as predicted by a robust (least-median-of-squares) regression derived from literature *in vivo* brain penetration data, and ADMET_AlogP98 is the octanol/water partition coefficient which is another key molecular characteristic for bioactive chemicals. Here, **1** showed low scores with both ADMET_BBB and ADMET_AlogP98 (Table S1, see Supporting

Information), which were in line with expectations. Among the evaluated DPCI analogues, **9**, **10**, **28**, **29**, **30**, **31** and **32** exhibited higher scores than **2**, **4**, **7**, **21**, **23**, **24**, **25** and **27** with 3',4'-dimethoxy substitutions in B ring, indicating that these analogues exhibited significantly enhanced lipophilicity which may contribute to improved permeability of these DPCIs.

To verify the prediction, we selected **28** as the representative compound for *in vitro* BBB penetration examination after a combined consideration of inhibitory activity, predicted ADMET_BBB score, and molecular weight, in which **28** and **30** were distinguished from others, but **30** is unfortunately less soluble in the test buffer. The *in vitro* BBB penetration was evaluated using a parallel artificial membrane permeation assay (PAMPA-BBB) following the generally reported protocols.[27-29] The UV/vis absorptions of **28** and **1** after permeating through a porcine polar brain lipid (PBL) membrane were recorded from 290 to 310 nm and the effective permeabilities (Pe) were calculated. As described in Figure 3, the Pe values of **28** in various wavelengths were significant higher than that of **1**, demonstrating a much stronger permeability of **28**. This result is consistent with our prediction.

Compound 28 inhibits QC and reduces generation of pE-Aβ_{3-42} in transfected HEK293T cells

Then, the hQC inhibitory potency of **28** was investigated in hQC and APP695 (NLQ) transfected human embryonal kidney cells HEK293T which over-express recombinant hQC and Aβ_{3-42}. It was found that **28** had no effect on the expression of hQC in transfected HEK293T cells (data not shown), but the activity of cellular hQC was effectively blocked by addition of **28** in the culture at a concentration of 10 μM. The percentage inhibition increased along with the culture time, and a maximal percentage inhibition was obtained after 24 h incubation (Figure 4A). Noticeably, when the culture time was extended to 48 h, a decreased percentage inhibition was observed, which could be attributed to a change in the expression and activity of recombinant hQC protein in the cell cycle different stages. The transfected HEK293T cells were therefore incubated with different concentrations of **28** for 24 h (Figure 4B), and a significant dose-dependent inhibition was observed as expected, which is associated with the dose-dependent decreased generation of pE-Aβ_{3-42} as determined by

ELISA (Figure 4C). These results indicated that **28** prevents the generation of pE-Aβ_{3-42} by the inhibition of hQC in cultured cells.

Compound 28 inhibits QC, reduces generation of pE-Aβ_{3-42} and improves the behavior of B6C3-Tg mice

Based on the above results of **28** on the hQC inhibition at both molecular and cellular levels, we would expect it to exhibit beneficial effects on AD pathogenesis by inhibiting the activity of QC and reducing the generation of toxic pE-Aβ_{3-42} *in vivo*. Therefore, compound **28** was applied to 3-month-old female B6C3-Tg mice for 2 months by intraperitoneal injection with two doses, L and H (2 and 10 mg per kg weight respectively). QC activity assay revealed a dose-dependent decrease of QC activity in the hippocampus, cortex and total brain of the **28** treated mice, respectively (Figure 5A and B, $P < 0.05$), which is associated with the dose-dependent decrease of pE-Aβ_{3-42} as revealed by ELISA (Figure 5C) and immunohistochemistry (Figure 5E and F). Interestingly, the accumulation of total soluble Aβs in the AD brain increased dose-dependently after the treatment of **28** (Figure 5D), which is attributed to the low conversion of normal Aβs to pE-Aβs caused by QC inhibition. As pE-Aβs are believed to serve as seed and promote the formation of Aβ plaques, especially in the early stage, the significant dose-dependent reduction of Aβ plaques (Figure 5G and H) may also resulted from the inhibition of pE-Aβs generation by **28** treatment.

Subsequently, compound **28** treatment resulted in a significant behavioral improvement in B6C3-tg mice as measured by a Nest-building test, reported as a useful index of behavioral deficits.[30, 31] Compared with the mice in control group, compound **28**-treated mice exhibited an obvious improvement in nest-building capacity (Figure 5I and S1, see Supporting Information). These findings validated that the QC inhibitor **28** specifically blocks the generation of pE-Aβs, reduces the Aβ plaques in AD brain, and finally improves function in B6C3-Tg mice by inhibiting the activity of QC.

CONCLUSIONS

QC is a new target for the development of novel drugs for the prevention and treatment of AD because

of the positive correlation between the expression of QC in the brain and the course of AD. Based on rational design, a new series of DPCIs were prepared. These chemicals with enhanced inflexibility and hydrophobicity exhibited powerful hQC inhibitory potency *in vitro* as expected. Fifteen compounds were more potent than the positive control, and the improved permeability of several was also confirmed by *in silico* and *in vitro* assays. In particular, the selected compound **28** showed remarkable inhibitory activities in a dose- and time- dependent manner in APP transfected HEK293T model cells. Treatment with **28** significantly decreased the generation of pE-A$\beta_{3\text{-}42}$ in living cells and inhibited the activity of hQC without interfering with its expression. Inhibitory efficacy was further validated in animal studies by intraperitoneal injections of **28** in B6C3-Tg AD mice. The inhibitory effect of **28** *in vivo* improved nest-building behavior, an index of functional deficits in these AD model mice. We believe these compounds represented a new class of hQC inhibitors that can contribute to the development of novel anti-AD agents. Further efforts toward revealing in the depth mechanism and activity of these inhibitors are now the focus of our ongoing investigations.

EXPERIMENTAL SECTION

The ^{1}H-NMR (400 MHz) data and ^{13}C-NMR (100 MHz) was recorded on a Bruker Avance III, using $CDCl_3$ as solvent. The high-resolution positive ion electrospray mass spectra were obtained from a LCMS-IT-TOF (SHIMADZU). Thin-layer chromatography (TLC) was performed on Merck silica gel $60F_{254}$ plates, and visualized with UV. Flash column chromatography was performed using silica gel (200-300 mesh, Qingdao Haiyang Chemical Co. Ltd, China). Purities of the final compounds used for biological evaluation were determined as above 95 % by HPLC/UV criteria (Agilent 1200). The porcine polar brain lipid (PBL) was purchased from Avanti Polar Lipids, Inc., USA. SensoLyte® green glutaminyl cyclase activity assay kit was purchased from AnaSpec, Inc. Amyloid-beta (N3pE-42) ELISA kit was purchased from IBL International, Germany. Monoclonal anti-β-amyloid protein (mouse IgG1 isotype) was purchased from Sigma, USA. Monoclonal mouse antibody against Aβ-pE3 was purchased from Synaptic Systems GmbH, Germany. Other materials were purchased from Alfa Aesar

Co. All other reagents were of analytical grade.

General procedure for the preparation of compounds 2-41.

(1) To a solution of bromaniline or derivatives (1 equiv) and phenylboronic acid or derivatives (1.2 equiv) in 1,4-dioxane (10 mL), $Pd(DPPF)_2Cl_2$ (0.06 equiv) and K_2CO_3 solution (2 mol/L, 10 mL) were added. Under an atmosphere of Ar the mixture was warmed to 100 °C. After 3h the reaction was quenched with a saturated NaCl solution (1 mL). The reaction mixture was extracted using ethyl acetate (20 mL × 3). The combined organic phase was washed with saturated NaCl solution, dried with anhydrous Na_2SO_4, filtered, and concentrated under reduced pressure. The residue was purified using flash column chromatography (silica gel, ethyl acetate/hexane, gradient elution) to provide the intermediate **i**.

(2) To intermediate **i** (1 equiv) in anhydrous acetonitrile (6 mL), 1,3-dibromopropane or 1,2-dibromoethane (7 equiv) and anhydrous K_2CO_3 (2 equiv) was added; the mixture was warmed and refluxed overnight. When cooled to room temperature, the acetonitrile was removed under reduced pressure, water (20 mL) was added, and the water phase was extracted using ethyl acetate (20 mL × 3). The combined organic phase was washed with saturated NaCl solution, dried with anhydrous Na_2SO_4, filtered, and concentrated under reduced pressure. The residue was purified using flash column chromatography (silica gel, ethyl acetate/hexane, gradient elution) to provide the intermediate **ii**.

(3) The nucleophile substitution reaction of **ii** (1 equiv) and imidazoles (1 equiv) provided the designed inhibitors according to the procedure in (2).

N-(3-(1H-Imidazol-1-yl)propyl)-3',4'-dimethoxy-[1,1'-biphenyl]-2-amine (**2**). Yield: 26%; ^{1}H NMR (400 MHz, $CDCl_3$): δ 1.97-2.06 (m, 2H, CH_2), 3.08-3.12 (m, 2H, CH_2), 3.88 (s, 3H, OCH_3), 3.93 (s, 3H, OCH_3), 3.97-4.01 (m, 2H, CH_2), 6.62-6.64 (d, J = 8.113 Hz, 1H, ArH), 6.76-6.81 (m, 1H, ArH), 6.86 (s, 1H, ArH), 6.91 (s, 1H, ArH), 6.95 (m, 2H, ArH), 7.06 (s, 1H, ArH), 7.09-7.12 (m, 1H, ArH), 7.20-7.23 (m, 1H, ArH), 7.26 (s, solv), 7.42 (s, 1H, ArH). ^{13}C NMR (100 MHz, $CDCl_3$): δ 30.71, 40.83, 44.48, 56.02, 110.51, 111.83, 112.96, 117.48, 118.74, 121.45, 127.96, 129.60, 130.30, 131.86, 137.08,

144.77, 148.54, 149.44. HRMS (EI): calculated for $C_{20}H_{23}N_3O_2$, 337.1790; found, $C_{20}H_{24}N_3O_2$, 338.1860 $[M+H]^+$.

N-(3-(1H-Imidazol-1-yl)propyl)-3',4'-dimethoxy-3-methyl-[1,1'-biphenyl]-2-amine (**3**). Yield: 13%; ^{1}H NMR (400 MHz, $CDCl_3$): δ 1.79-1.85 (m, 2H, CH_2), 2.31 (s, 3H, CH_3), 2.81-2.85 (t, *J* = 13.663 Hz, 2H, CH_2), 3.81-3.85 (t, *J* = 14.033 Hz, 2H, CH_2), 3.88 (s, 3H, OCH_3), 3.95 (s, 3H, OCH_3), 6.76 (s, 1H, ArH), 6.93-6.97 (m, 4H, ArH), 7.03-7.07 (m, 2H, ArH), 7.13-7.15 (d, *J* = 7.123 Hz, 1H, ArH), 7.28 (s, solv), 7.33 (s, 1H, ArH). ^{13}C NMR (100 MHz, $CDCl_3$): δ 18.86, 32.10, 44.50, 45.22, 55.97, 111.36, 112.43, 112.59, 118.66, 121.11, 121.46, 128.70, 128.93, 129.38, 130.56, 133.19, 133.61, 144.51, 148.25, 148.96. HRMS (EI): calcd for $C_{21}H_{25}N_3O_2$, 351.1947; found, $C_{21}H_{26}N_3O_2$, 352.2025 $[M+H]^+$.

N-(3-(1H-Imidazol-1-yl)propyl)-3-fluoro-3',4'-dimethoxy-[1,1'-biphenyl]-2-amine (**4**). Yield: 33%; ^{1}H NMR (400 MHz, $CDCl_3$): δ 1.85-1.91 (m, 2H, CH_2), 3.04-3.07 (t, *J* = 13.368 Hz, 2H, CH_2), 3.87-3.91 (m, 5H, CH_2, OCH_3), 3.95 (s, 3H, OCH_3), 6.79 (s, 1H, ArH), 6.83-6.87 (m, 1H, ArH), 6.92 (s, 1H, ArH), 6.94-6.96 (m, 2H, ArH), 6.98-6.99 (m, 1H, ArH), 7.01-7.04 (m, 2H, ArH), 7.28 (s, solv), 7.33 (s, 1H, ArH). ^{13}C NMR (100 MHz, $CDCl_3$): δ 32.00, 44.00, 44.24, 56.00, 111.51, 112.24, 115.04, 115.25, 118.64, 119.94, 121.11, 126.17, 128.52, 131.30, 133.27, 133.79, 136.99, 148.65, 149.20. HRMS (EI): calcd for $C_{20}H_{22}FN_3O_2$, 355.1696; found, $C_{20}H_{23}FN_3O_2$, 356.1769 $[M+H]^+$.

N-(3-(1H-Imidazol-1-yl)propyl)-3',4'-dimethoxy-4-methyl-[1,1'-biphenyl]-2-amine (**5**). Yield: 14.6%; ^{1}H NMR (400 MHz, $CDCl_3$): δ 2.01-2.07 (m, 2H, CH_2), 2.36 (s, 3H, CH_3), 3.11-3.14 (m, 2H, CH_2), 3.89 (s, 3H, OCH_3), 3.95 (s, 3H, OCH_3), 4.00-4.03 (m, 2H, CH_2), 6.47 (s, 1H, ArH), 6.63-6.65 (d, *J* = 7.916 Hz, 1H, ArH), 6.89 (s, 1H, ArH), 6.92 (s, 1H, ArH), 6.95-6.96 (m, 2H, ArH), 7.01-7.03 (d, *J* = 7.916 Hz, 1H, ArH), 7.08 (s, 1H, ArH), 7.28 (s, solv), 7.46 (s, 1H, ArH). ^{13}C NMR (100 MHz, $CDCl_3$): δ 21.67, 30.69, 40.72, 44.45, 55.96, 111.25, 111.58, 112.83, 118.19, 118.77, 121.45, 125.20, 129.62, 130.17, 131.76, 137.12, 138.52, 144.60, 148.27, 149.25. HRMS (EI): calcd for $C_{21}H_{25}N_3O_2$, 351.1947; found, $C_{21}H_{26}N_3O_2$, 352.2020 $[M+H]^+$.

N-(3-(1H-Imidazol-1-yl)propyl)-5-isopropyl-3',4'-dimethoxy-[1,1'-biphenyl]-2-amine (**6**). Yield:

15%; ^{1}H NMR (400 MHz, $CDCl_3$): δ 1.25 (s, 3H, CH_3), 1.27 (s, 3H, CH_3), 2.01-2.05 (t, *J* = 13.620 Hz, 2H, CH_2), 2.83-2.90 (m, 1H, CH), 3.10-3.13 (t, *J* = 13.439 Hz, 2H, CH_2), 3.91 (s, 3H, OCH_3), 3.96 (s, 3H, OCH_3), 4.00-4.03 (t, *J* = 13.894 Hz, 2H, CH_2), 6.60-6.62 (d, *J* = 8.350 Hz, 1H, ArH), 6.89 (s, 1H, ArH), 6.95 (s, 1H, ArH), 6.98-7.11 (m, 3H, ArH), 7.11 (s, 1H, ArH), 7.11-7.13 (d, *J* = 10.66 Hz, 1H, ArH), 7.28 (s, solv), 7.45 (s, 1H, ArH). ^{13}C NMR (100 MHz, $CDCl_3$): δ 24.23, 30.76, 33.16, 41.03, 44.56, 56.00, 110.61, 111.57, 112.76, 118.84, 121.45, 126.29, 127.86, 128.50, 129.24, 132.09, 137.02, 138.01, 142.76, 148.33, 149.21. HRMS (EI): calcd for $C_{23}H_{29}N_3O_2$, 379.2260; found, $C_{23}H_{30}N_3O_2$, 380.2334 $[M+H]^+$.

N-(3-(1H-Imidazol-1-yl)propyl)-3',4'-dimethoxy-6-methyl-[1,1'-biphenyl]-2-amine (**7**). Yield: 14%; ^{1}H NMR (400 MHz, $CDCl_3$): δ 1.96-1.99 (t, *J* = 13.494 Hz, 2H, CH_2), 2.03 (s, 3H, CH_3), 3.06-3.09 (t, *J* = 13.465 Hz, 2H, CH_2), 3.87 (s, 3H, OCH_3), 3.93-3.96 (m, 5H, CH_2, OCH_3), 6.50-6.52 (d, *J* = 8.295 Hz, 1H, ArH), 6.69-6.71 (d, *J* = 7.585 Hz, 1H, ArH), 6.75-6.80 (m, 2H, ArH), 6.85 (s, 1H, ArH), 7.00-7.02 (d, *J* = 8.014 Hz, 1H, ArH), 7.06 (s, 1H, ArH), 7.14-7.18 (t, *J* = 15.472 Hz, 1H, ArH), 7.28 (s, solv), 7.40 (s,1H, ArH). ^{13}C NMR (100 MHz, $CDCl_3$): δ 20.65, 30.56, 40.65, 44.33, 55.99, 107.78, 111.94, 113.08, 118.74, 119.09, 122.07, 127.55, 128.23, 129.62, 130.21, 137.09, 137.15, 145.37, 148.28, 149.66. HRMS (EI): calcd for $C_{21}H_{25}N_3O_2$, 351.1947; found, $C_{21}H_{26}N_3O_2$, 352.2024 $[M+H]^+$.

N-(3-(1H-Imidazol-1-yl)propyl)-4'-fluoro-[1,1'-biphenyl]-2-amine (**8**). Yield: 22%; ^{1}H NMR (400 MHz, $CDCl_3$): δ 1.99-2.06 (m, 2H, CH_2), 3.09-3.12 (t, *J* = 13.178 Hz, 2H, CH_2), 3.71 (s, 1H, NH), 3.98-4.01 (t, *J* = 13.868 Hz, 2H, CH_2), 6.63-6.65 (d, *J* = 8.241 Hz, 1H, ArH), 6.77-6.81 (m, 1H, ArH), 6.86 (s, 1H, ArH), 7.05-7.08 (m, 2H, ArH), 7.12-7.17 (t, *J* = 17.530 Hz, 2H, ArH), 7.22-7.24 (m, 1H, ArH), 7.26 (s, solv), 7.34-7.38 (m, 2H, ArH), 7.41 (s, 1H, ArH). ^{13}C NMR (100 MHz, $CDCl_3$): δ 30.61, 40.72, 44.42, 110.53, 115.84, 116.05, 117.58, 118.71, 126.97, 128.97, 129.78, 130.43, 130.97, 135.09, 137.11, 144.59, 160.93, 163.38. HRMS (EI): calcd for $C_{18}H_{18}FN_3$, 295.1485; found, $C_{18}H_{19}FN_3$, 296.1556 $[M+H]^+$.

N-(3-(1H-Imidazol-1-yl)propyl)-4'-fluoro-6-methyl-[1,1'-biphenyl]-2-amine (**9**). Yield: 13%; ^{1}H

NMR (400 MHz, $CDCl_3$): δ 1.96-2.00 (m, 5H, CH_2, CH_3), 3.06-3.09 (t, J = 13.147 Hz, 2H, CH_2), 3.93-3.97 (t, J = 13.878 Hz, 2H, CH_2), 6.50-6.52 (d, J = 7.950 Hz, 1H, ArH), 6.69-6.71 (d, J = 7.666 Hz, 1H, ArH), 6.85 (s, 1H, ArH), 7.06 (s, 1H, ArH), 7.15-7.21 (m, 5H, ArH), 7.28 (s, solv), 7.41 (s, 1H, ArH). ^{13}C NMR (100 MHz, $CDCl_3$): δ 20.70, 30.48, 40.58, 44.34, 107.85, 116.31, 116.52, 118.74, 119.23, 126.60, 128.48, 129.62, 131.77, 131.84, 133.67, 137.01, 145.12, 160.96, 163.41. HRMS (EI): calcd for $C_{19}H_{20}FN_3$, 309.1641; found, $C_{19}H_{21}FN_3$, 310.1714 $[M+H]^+$.

N-(3-(1H-Imidazol-1-yl)propyl)-4',6-difluoro-[1,1'-biphenyl]-2-amine (**10**). Yield: 15%; ^{1}H NMR (400 MHz, $CDCl_3$): δ 1.98-2.04 (m, 2H, CH_2), 3.08-3.11 (t, J = 13.455 Hz, 2H, CH_2), 3.60 (s, 1H, NH), 3.97-4.00 (t, J = 13.491 Hz, 2H, CH_2), 6.39-6.41 (d, J = 8.197 Hz, 1H, ArH), 6.51-6.55 (t, J = 17.335 Hz, 1H, ArH), 6.86 (s, 1H, ArH), 7.07 (s, 1H, ArH), 7.15-7.20 (m, 3H, ArH), 7.27 (s, solv), 7.29-7.32 (m, 2H, ArH), 7.50 (s, 1H, ArH). ^{13}C NMR (100 MHz, $CDCl_3$): δ 30.46, 40.79, 44.48, 104.44, 104.63, 105.89, 116.16, 116.33, 118.75, 127.87, 129.36, 129.63, 129.71, 132.18, 132.24, 146.63, 161.54, 163.51. HRMS (EI): calcd for $C_{18}H_{17}F_2N_3$, 313.1391; found, $C_{18}H_{18}F_2N_3$, 314.1464 $[M+H]^+$.

N-(3-(1H-Imidazol-1-yl)propyl)-3'-fluoro-[1,1'-biphenyl]-2-amine (**11**). Yield: 17%; ^{1}H NMR (400 MHz, $CDCl_3$): δ 2.01-2.05 (m, 2H, CH_2), 3.09-3.11 (t, J = 13.490 Hz, 2H, CH_2), 3.73 (s, 1H, NH), 3.98-4.00 (t, J = 14.156 Hz, 2H, CH_2), 6.63-6.64 (d, J = 8.150 Hz, 1H, ArH), 6.77-6.80 (t, J = 15.640 Hz, 1H, ArH), 6.86 (s, 1H, ArH), 7.04-7.08 (m, 3H, ArH), 7.10-7.12 (d, J = 8.440 Hz, 1H, ArH), 7.17-7.18 (d, J = 7.599 Hz, 1H, ArH), 7.22-7.25 (t, J = 17.061 Hz, 1H, ArH), 7.27 (s, solv), 7.29-7.43 (m, 2H, ArH). ^{13}C NMR (100 MHz, $CDCl_3$): δ 30.53, 40.64, 44.52, 110.62, 114.24, 114.45, 116.20, 116.41, 117.60, 124.99, 126.64, 129.24, 130.27, 130.51, 141.55, 144.36, 161.86, 164.32. HRMS (EI): calcd for $C_{18}H_{18}FN_3$, 295.1485; found, $C_{18}H_{19}FN_3$, 296.1559 $[M+H]^+$.

3',4'-Dimethoxy-3-methyl-N-(3-(2-methyl-1H-imidazol-1-yl)propyl)-[1,1'-biphenyl]-2-amine (**12**). Yield: 14%; ^{1}H NMR (400 MHz, $CDCl_3$): δ 1.92-1.96 (m, 2H, CH_2), 2.03 (s, 3H, CH_3), 2.21 (s, 3H, CH_3), 3.05-3.09 (m, 2H, CH_2), 3.84-3.89 (m, 5H, CH_2, OCH_3), 3.96 (s, 3H, OCH_3), 6.50-6.55 (m, 2H, ArH), 6.68-6.70 (d, J = 7.306 Hz, 1H, ArH), 6.74-6.75 (d, J = 1.965 Hz, 1H, ArH), 6.77-6.79 (m, 1H,

ArH), 6.99-7.02 (m, 1H, ArH), 7.14-7.18 (t, *J* = 15.688 Hz, 1H,), 7.28 (s, solv), 7.31 (s, 1H, ArH). ^{13}C NMR (100 MHz, $CDCl_3$): δ 12.80, 18.89, 31.66, 43.63, 45.31, 55.96, 111.27, 112.35, 118.82, 121.08, 121.38, 126.88, 128.75, 128.77, 130.54, 133.21, 133.41, 144.22, 144.55, 148.19, 148.90. HRMS (EI): calcd for $C_{22}H_{27}N_3O_2$, 365.2103; found, $C_{22}H_{28}N_3O_2$, 366.2177 $[M+H]^+$.

3',4'-Dimethoxy-4-methyl-N-(3-(2-methyl-1H-imidazol-1-yl)propyl)-[1,1'-biphenyl]-2-amine (**13**). Yield: 17%; ^{1}H NMR (400 MHz, $CDCl_3$): δ 1.77-1.80 (m, 2H, CH_2), 2.20 (s, 3H, CH_3), 2.31 (s, 3H, CH_3), 2.81-2.84 (m, 2H, CH_2), 3.73-3.76 (m, 2H, CH_2), 3.88 (s, 3H, OCH_3), 3.95 (s, 3H, OCH_3), 6.46 (s, 1H, ArH), 6.91-6.96 (m, 4H, ArH), 7.05-7.06 (d, *J* = 7.487 Hz, 1H, ArH), 7.12-7.14 (d, *J* = 7.113 Hz, 1H, ArH), 7.21 (s, 1H, ArH), 7.28(s, solv). ^{13}C NMR (100 MHz, $CDCl_3$): δ 13.57, 18.88, 32.06, 44.40, 45.25, 55.95, 111.34, 112.42, 112.43, 115.12, 121.12, 121.39, 128.69, 128.76, 128.89, 130.55, 133.22, 133.53, 144.55, 148.24, 148.95. HRMS m/z: calcd for $C_{22}H_{27}N_3O_2$, 365.2103; found, $C_{22}H_{28}N_3O_2$, 366.2177 $[M+H]^+$.

5-Isopropyl-3',4'-dimethoxy-N-(3-(2-methyl-1H-imidazol-1-yl)propyl)-[1,1'-biphenyl]-2-amine (**14**). Yield: 20%; ^{1}H NMR (400 MHz, $CDCl_3$): δ 1.25 (s, 3H, CH_3), 1.27 (s, 3H, CH_3), 1.96-2.03 (m, 2H, CH_2), 2.22 (s, 3H, CH_3), 2.83-2.90 (m, 1H, CH), 3.09-3.12 (t, *J* = 13.434 Hz, 2H, CH_2), 3.88-3.93 (m, 5H, CH_2, OCH_3), 3.96 (s, 3H, OCH_3), 6.58-6.63 (m, 2H, ArH), 6.96 (s, 1H, ArH), 6.98 (s, 2H, ArH), 7.00-7.01 (d, *J* = 2.226 Hz, 1H, ArH), 7.11-7.14 (m, 1H, ArH), 7.28 (s, solv), 7.31 (s, 1H, ArH). ^{13}C NMR (100 MHz, $CDCl_3$): δ 12.64, 23.22, 29.72, 32.15, 40.04, 43.30, 54.98, 109.60, 110.55, 111.75, 114.22, 120.45, 125.27, 126.80, 127.46, 131.11, 135.20, 136.91, 137.63, 141.81, 147.31, 148.20. HRMS (EI): calcd for $C_{24}H_{31}N_3O_2$, 393.2416; found, $C_{24}H_{32}N_3O_2$, 394.2486 $[M+H]^+$.

4'-Fluoro-N-(3-(2-methyl-1H-imidazol-1-yl)propyl)-[1,1'-biphenyl]-2-amine (**15**). Yield: 32%; ^{1}H NMR (400 MHz, $CDCl_3$): δ 1.94-2.00 (m, 2H, CH_2), 2.31 (s, 3H, CH_3), 3.11 (s, 2H, CH_2), 3.69 (s, 1H, NH), 3.87-3.90 (t, *J* = 13.833 Hz, 2H, CH_2), 6.62-6.64 (d, *J* = 7.880 Hz, 1H, ArH), 6.75-6.76 (d, *J* = 1.360 Hz, 1H, ArH), 6.78-6.81 (t, *J* = 15.721 Hz, 1H, ArH), 6.90 (s, 1H, ArH), 7.06-7.08 (m, 1H, ArH), 7.12-7.16 (t, *J* = 17.136 Hz, 2H, ArH), 7.22-7.24 (m, 1H, ArH), 7.26 (s, solv), 7.34-7.38 (m, 2H, ArH).

^{13}C NMR (100 MHz, $CDCl_3$): δ 12.92, 30.29, 40.68, 43.42, 110.50, 115.82, 116.03, 117.59, 118.89, 125.97, 127.44, 128.97, 130.40, 130.97, 131.05, 135.11, 144.60, 160.93, 163.38. HRMS (EI): calcd for $C_{19}H_{20}FN_3$, 309.1641; found, $C_{19}H_{21}FN_3$, 310.1715 $[M+H]^+$.

4'-Fluoro-6-methyl-N-(3-(2-methyl-1H-imidazol-1-yl)propyl)-[1,1'-biphenyl]-2-amine (**16**). Yield: 13%; ^{1}H NMR (400 MHz, $CDCl_3$): δ 1.89-1.96 (m, 2H, CH_2), 1.99 (s, 3H, CH_3), 2.30 (s, 3H, CH_3), 3.06-3.10 (t, *J* = 13.097 Hz, 2H, CH_2), 3.82-3.86 (t, *J* = 13.692 Hz, 2H, CH_2), 6.50-6.52 (d, *J* = 8.169 Hz, 1H, ArH), 6.69-6.71 (d, *J* = 7.495 Hz, 1H, ArH), 6.73-6.74 (d, *J* = 1.361 Hz, 1H, ArH), 6.91 (s, 1H, ArH), 7.15-7.21 (m, 5H, ArH), 7.28 (s, solv). ^{13}C NMR (100 MHz, $CDCl_3$): δ 12.87, 20.70, 30.21, 40.54, 43.32, 107.80, 116.30, 116.51, 118.90, 119.24, 126.59, 127.28, 128.49, 131.77, 131.85, 133.65, 136.98, 145.15, 160.95, 166.28. HRMS (EI): calcd for $C_{20}H_{22}FN_3$, 323.1798; found, $C_{20}H_{23}FN_3$, 324.1873 $[M+H]^+$.

4',6-Difluoro-N-(3-(2-methyl-1H-imidazol-1-yl)propyl)-[1,1'-biphenyl]-2-amine (**17**). Yield: 20%; ^{1}H NMR (400 MHz, $CDCl_3$): δ 1.94-2.00 (m, 2H, CH_2), 2.37 (s, 3H, CH_3), 3.12 (s, 2H, CH_2), 3.61 (s, 1H, NH), 3.87-3.90 (t, *J* = 14.039 Hz, 2H, CH_2), 6.40-6.42 (d, *J* = 8.199 Hz, 1H, ArH), 6.52-6.57 (t, *J* = 17.440 Hz, 1H, ArH), 6.77 (s, 1H, ArH), 6.95 (s, 1H, ArH), 7.17-7.22 (m, 3H, ArH), 7.28 (s, solv), 7.30-7.33 (m, 2H, ArH). ^{13}C NMR (100 MHz, $CDCl_3$): δ 12.66, 30.07, 40.70, 43.53, 104.52, 104.70, 105.86, 116.17, 116.34, 118.94, 127.84, 129.66, 129.75, 132.17, 132.24, 146.59, 159.47, 161.54, 163.51. HRMS (EI): calcd for $C_{19}H_{19}F_2N_3$, 327.1547; found, $C_{19}H_{20}F_2N_3$, 328.1624 $[M+H]^+$.

4'-Fluoro-4-methyl-N-(3-(2-methyl-1H-imidazol-1-yl)propyl)-[1,1'-biphenyl]-2-amine (**18**). Yield: 15%; ^{1}H NMR (400 MHz, $CDCl_3$): δ 2.01-2.04 (m, 2H, CH_2), 2.19 (s, 3H, CH_3), 2.35 (s, 3H, CH_3), 3.11-3.13 (t, *J* = 13.519 Hz, 2H, CH_2), 3.95-3.98 (t, *J* = 13.846 Hz, 2H, CH_2), 6.45 (s, 1H, ArH), 6.62-6.64 (d, *J* = 7.860 Hz, 2H, ArH), 6.96-6.97 (d, *J* = 7.482 Hz, 1H, ArH), 7.12-7.15 (t, *J* = 17.449 Hz, 3H, ArH), 7.27 (s, solv), 7.33-7.35 (m, 2H, ArH). ^{13}C NMR (100 MHz, $CDCl_3$): δ 12.87, 20.70, 30.21, 40.54, 43.32, 107.80, 116.30, 116.51, 118.90, 119.24, 125.59, 127.28, 128.49, 131.77, 131.85, 133.65, 133.68, 136.98, 145.15, 160.95. HRMS (EI): calcd for $C_{20}H_{22}FN_3$, 323.1798; found, $C_{20}H_{23}FN_3$,

324.1872 $[M+H]^+$.

3'-Fluoro-N-(3-(2-methyl-1H-imidazol-1-yl)propyl)-[1,1'-biphenyl]-2-amine (**19**). Yield: 19%; ^{1}H NMR (400 MHz, $CDCl_3$): δ 1.98-2.02 (m, 2H, CH_2), 2.20 (s, 3H, CH_3), 3.08-3.11 (t, *J* = 13.664 Hz, 2H, CH_2), 3.90-3.93 (t, *J* = 13.674 Hz, 2H, CH_2), 6.57 (s, 1H, ArH), 6.64-6.65 (d, *J* = 2.014 Hz, 1H, ArH), 6.76-6.81 (m, 1H, ArH), 7.05-7.09 (m, 2H, ArH), 7.11-7.13 (d, *J* = 5.998 Hz, 1H, ArH), 7.17-7.19 (d, *J* = 6.014 Hz, 1H, ArH), 7.23-7.25 (d, *J* = 5.875 Hz, 1H, ArH), 7.26 (s, solv), 7.31 (s, 1H, ArH), 7.39-7.44 (m, 1H, ArH). ^{13}C NMR (100 MHz, $CDCl_3$): δ 12.75, 30.21, 40.58, 43.51, 110.60, 114.25, 114.46, 116.21, 116.42, 117.67, 118.95, 125.00, 126.87, 129.25, 130.26, 130.51, 144.34, 161.85, 164.31. HRMS (EI): calcd for $C_{19}H_{20}FN_3$, 309.1641; found, $C_{19}H_{21}FN_3$, 310.1709 $[M+H]^+$.

3'-Fluoro-5-isopropyl-N-(3-(2-methyl-1H-imidazol-1-yl)propyl)-[1,1'-biphenyl]-2-amine (**20**). Yield: 19%; ^{1}H NMR (400 MHz, $CDCl_3$): δ 1.22 (s, 3H, CH_3), 1.24 (s, 3H, CH_3), 1.93-2.01 (m, 2H, CH_2), 2.35 (s, 3H, CH_3), 2.80-2.89 (m, 1H, CH), 3.08-3.13 (t, *J* = 13.007 Hz, 2H, CH_2), 3.88-3.93 (t, *J* = 13.996 Hz, 2H, CH_2), 6.58-6.61 (d, *J* = 8.203 Hz, 1H, ArH), 6.78 (s, 1H, ArH), 6.93 (s, 1H,), 6.96-6.97 (d, *J* = 2.190 Hz, 1H, ArH), 7.03-7.21 (m, 4H, ArH), 7.26 (s, solv), 7.38-7.45 (m, 1H, ArH). ^{13}C NMR (100 MHz, $CDCl_3$): δ 12.61, 24.14, 30.35, 33.13, 40.95, 43.59, 108.51, 110.89, 114.11, 116.25, 116.41, 118.94, 125.01, 125.95, 128.39, 130.45, 138.34, 142.37, 162.11, 164.07. HRMS (EI): calcd for $C_{22}H_{26}FN_3$, 351.2111; found, $C_{22}H_{27}FN_3$, 352.2184 $[M+H]^+$.

3',4'-Dimethoxy-N-(3-(4-methyl-1H-imidazol-1-yl)propyl)-[1,1'-biphenyl]-2-amine (**21**). Yield: 19%; ^{1}H NMR (400 MHz, $CDCl_3$): δ 1.94-2.03 (m, 2H, CH_2), 2.20 (s, 3H, CH_3), 3.07-3.12 (m, 2H, CH_2), 3.83-3.91 (m, 5H, CH_2, OCH_3), 3.93 (s, 3H, OCH_3), 6.56 (s, 1H, ArH), 6.62-6.65 (d, *J* = 7.996 Hz, 1H, ArH), 6.76-6.81 (m, 1H, ArH), 6.91 (s, 1H, ArH), 6.95 (s, 2H, ArH), 7.09-7.12 (dd, *J* = 9.012 Hz, 1H, ArH), 7.20-7.22 (m, 1H, ArH), 7.26 (s, solv), 7.31 (s, 1H, ArH). ^{13}C NMR (100 MHz, $CDCl_3$): δ 12.84, 30.32, 40.69, 43.44, 55.98, 110.41, 111.57, 112.72, 117.45, 118.92, 121.39, 127.20, 127.88, 128.64, 130.27, 130.56, 131.72, 144.74, 148.39, 149.29. HRMS (EI): calcd for $C_{21}H_{25}N_3O_2$, 351.1947; found, $C_{21}H_{26}N_3O_2$, 352.2023 $[M+H]^+$.

3',4'-Dimethoxy-3-methyl-N-(3-(4-methyl-1H-imidazol-1-yl)propyl)-[1,1'-biphenyl]-2-amine (**22**). Yield: 14%; ^{1}H NMR (400 MHz, $CDCl_3$): δ 1.76-1.80 (m, 2H, CH_2), 2.20 (s, 3H, CH_3), 2.31 (s, 3H, CH_3), 2.81-2.84 (t, *J* = 14.081 Hz, 2H, CH_2), 3.73-3.76 (t, *J* = 13.765 Hz, 2H, CH_2), 3.88 (s, 3H, OCH_3), 3.95 (s, 3H, OCH_3), 6.46 (s, 1H, ArH), 6.93-6.95 (m, 4H, ArH), 7.05-7.06 (d, *J* = 7.373 Hz, 1H, ArH), 7.12-7.14 (d, *J* = 7.145 Hz, 1H, ArH), 7.21 (s, 1H, ArH), 7.28 (s, solv). ^{13}C NMR (100 MHz, $CDCl_3$): δ 13.57, 18.88, 32.06, 44.40, 45.25, 55.97, 111.34, 112.43, 115.12, 121.12, 121.39, 128.69, 128.75, 128.89, 130.53, 130.55, 133.22, 133.53, 144.55, 148.24, 148.95. HRMS (EI): calcd for $C_{22}H_{27}N_3O_2$, 365.2103; found, $C_{22}H_{28}N_3O_2$, 366.2179 $[M+H]^+$.

3-Fluoro-3',4'-dimethoxy-N-(3-(4-methyl-1H-imidazol-1-yl)propyl)-[1,1'-biphenyl]-2-amine (**23**). Yield: 22%; ^{1}H NMR (400 MHz, $CDCl_3$): δ 1.80-1.88 (m, 2H, CH_2), 2.20 (s, 3H, CH_3), 3.03-3.06 (t, *J* = 13.102 Hz, 2H, CH_2), 3.79-3.82 (t, *J* = 14.252 Hz, 2H, CH_2), 3.89 (s, 3H, OCH_3), 3.95 (s, 3H, OCH_3), 6.48 (s, 1H, ArH), 6.82-6.87 (m, 1H, ArH), 6.92-6.96 (m, 4H, ArH), 6.98-7.04 (m, 1H, ArH), 7.20 (s, 1H, ArH), 7.28 (s, solv). ^{13}C NMR (100 MHz, $CDCl_3$): δ 13.63, 31.92, 44.01, 44.11, 55.97, 111.48, 112.25, 115.08, 115.24, 119.81, 119.89, 121.12, 126.15, 131.35, 133.19, 133.75, 136.07, 138.48, 148.64, 149.20. HRMS (EI): calcd for $C_{21}H_{24}FN_3O_2$, 369.1853; found, $C_{21}H_{25}FN_3O_2$, 370.1922 $[M+H]^+$.

3',4'-Dimethoxy-4-methyl-N-(3-(4-methyl-1H-imidazol-1-yl)propyl)-[1,1'-biphenyl]-2-amine (**24**). Yield: 15%; ^{1}H NMR (400 MHz, $CDCl_3$): δ 1.92-1.96 (m, 2H, CH_2), 2.03 (s, 3H, CH_3), 2.21 (s, 3H, CH_3), 3.05-3.09 (t, *J* = 13.564 Hz, 2H, CH_2), 3.84-3.89 (m, 5H, CH_2, OCH_3), 3.96 (s, 3H, OCH_3), 6.50-6.55 (m, 2H, ArH), 6.68-6.70 (d, *J* = 7.402 Hz, 1H, ArH), 6.74-6.75 (d, *J* = 1.866 Hz, 1H, ArH), 6.77-6.79 (m, 1H, ArH), 6.99-7.02 (dd, *J* = 10.143 Hz, 1H, ArH), 7.14-7.18 (t, *J* = 15.855 Hz, 1H, ArH), 7.28 (s, solv), 7.31 (s, 1H, ArH). ^{13}C NMR (100 MHz, $CDCl_3$): δ 13.56, 20.64, 30.47, 40.62, 44.23, 55.97, 107.76, 111.91, 113.07, 115.24, 119.00, 122.06, 127.49, 128.20, 130.20, 136.12, 137.10, 138.45, 145.38, 148.25, 149.62. HRMS (EI) m/z: calcd for $C_{22}H_{27}N_3O_2$, 365.2103; found, $C_{22}H_{28}N_3O_2$, 366.2179 $[M+H]^+$.

3',4'-Dimethoxy-5-methyl-N-(3-(4-methyl-1H-imidazol-1-yl)propyl)-[1,1'-biphenyl]-2-amine (**25**). Yield: 23%; ^{1}H NMR (400 MHz, $CDCl_3$): δ 1.95-2.02 (m, 2H, CH_2), 2.21 (s, 3H, CH_3), 2.29 (s, 3H, CH_3), 3.07-3.11 (t, *J* = 13.342 Hz, 2H, CH_2), 3.55-3.59 (t, *J* = 12.350 Hz, 2H, CH_2), 3.90 (s, 3H, OCH_3), 3.94 (s, 3H, OCH_3), 6.57-6.59 (d, *J* = 7.916 Hz, 2H, ArH), 6.92-6.96 (m, 4H, ArH), 7.04-7.06 (d, *J* = 8.041 Hz, 1H, ArH), 7.28(s, solv), 7.32(s, 1H, ArH). ^{13}C NMR (100 MHz, $CDCl_3$): δ 13.52, 20.31, 31.08, 34.88, 41.08, 55.97, 110.85, 111.54, 112.71, 115.30, 121.35, 125.63, 125.69, 127.97, 128.01, 128.96, 131.01, 131.90, 142.49, 148.32, 149.24. HRMS (EI): calcd for $C_{22}H_{27}N_3O_2$, 365.2103; found, $C_{22}H_{28}N_3O_2$, 366.2170 $[M+H]^+$.

5-Isopropyl-3',4'-dimethoxy-N-(3-(4-methyl-1H-imidazol-1-yl)propyl)-[1,1'-biphenyl]-2-amine (**26**). Yield: 17%; ^{1}H NMR (400 MHz, $CDCl_3$): δ 1.25 (s, 3H, CH_3), 1.27 (s, 3H, CH_3), 1.96-2.03 (m, 2H, CH_2), 2.22 (s, 3H, CH_3), 2.83-2.90 (m, 1H, CH), 3.09-3.12 (t, *J* = 13.614 Hz, 2H, CH_2), 3.88-3.93 (m, 5H, CH_2, OCH_3), 3.96 (s, 3H, OCH_3), 6.58-6.63 (m, 2H, ArH), 6.96 (s, 1H, ArH), 6.98 (m, 2H, ArH), 7.00-7.01 (d, *J* = 2.339 Hz, 1H, ArH), 7.11-7.14 (m, 1H, ArH), 7.28 (s, solv), 7.31 (s, 1H, ArH). ^{13}C NMR (100 MHz, $CDCl_3$): δ 12.64, 23.22, 29.72, 32.15, 40.04, 43.30, 54.98, 109.60, 110.55, 111.75, 114.22, 120.45, 125.27, 126.80, 127.46, 131.11, 135.20, 136.91, 137.63, 141.81, 147.31, 148.20. HRMS (EI): calcd for $C_{24}H_{31}N_3O_2$, 393.2416; found, $C_{24}H_{32}N_3O_2$, 394.2485 $[M+H]^+$.

3',4'-Dimethoxy-6-methyl-N-(3-(4-methyl-1H-imidazol-1-yl)propyl)-[1,1'-biphenyl]-2-amine (**27**). Yield: 15%; ^{1}H NMR (400 MHz, $CDCl_3$): δ 1.91-1.98 (m, 2H, CH_2), 2.03 (s, 3H, CH_3), 2.21 (s, 3H, CH_3), 3.06-3.09 (t, *J* = 13.551 Hz, 2H, CH_2), 3.84-3.88 (m, 5H, CH_2, CH_3), 3.96 (s, 3H, OCH_3), 6.50-6.55 (m, 2H, ArH), 6.68-6.70 (d, *J* = 7.335 Hz, 1H, ArH), 6.74-6.79 (m, 2H, ArH), 7.00-7.02 (d, *J* = 8.067 Hz, 1H, ArH), 7.14-7.18 (t, *J* = 15.845 Hz, 1H, ArH), 7.28 (s, solv), 7.31 (s, 1H, ArH). ^{13}C NMR (100 MHz, $CDCl_3$): δ 13.56, 20.64, 30.47, 40.62, 44.23, 55.90, 107.76, 111.91, 113.07, 115.24, 119.00, 122.06, 127.49, 128.20, 130.20, 135.12, 137.10, 138.45, 145.38, 148.25, 149.62. HRMS (EI): calcd for $C_{22}H_{27}N_3O_2$, 365.2103; found, $C_{22}H_{28}N_3O_2$, 366.2176 $[M+H]^+$.

4'-Fluoro-N-(3-(4-methyl-1H-imidazol-1-yl)propyl)-[1,1'-biphenyl]-2-amine (**28**). Yield: 26%; ^{1}H

NMR (400 MHz, $CDCl_3$): δ 1.98-2.02 (m, 2H, CH_2), 2.20 (s, 3H, CH_3), 3.08-3.11 (t, *J* = 13.381 Hz, 2H, CH_2), 3.90-3.93 (t, *J* = 14.287 Hz, 2H, CH_2), 6.57 (s, 1H, ArH), 6.63-6.65 (d, *J* = 8.270 Hz, 1H, ArH), 6.77-6.80 (t, *J* = 15.947 Hz, 2H, ArH), 7.05-7.07 (d, *J* = 8.703 Hz, 1H, ArH), 7.13-7.16 (t, *J* = 166.900 Hz, 2H, ArH), 7.22-7.25 (m, 1H, ArH), 7.26 (s, solv), 7.34-7.37 (m, 2H, ArH). ^{13}C NMR (100 MHz, $CDCl_3$): δ 13.54, 30.48, 40.72, 44.40, 110.54, 115.33, 115.77, 115.98, 117.45, 126.88, 128.91, 130.35, 130.93, 131.01, 136.13, 138.31, 144.61, 160.86, 163.31. HRMS (EI): calcd for $C_{19}H_{20}FN_3$, 309.1641; found, $C_{19}H_{21}FN_3$, 310.1716 $[M+H]^+$.

4'-Fluoro-4-methyl-N-(3-(4-methyl-1H-imidazol-1-yl)propyl)-[1,1'-biphenyl]-2-amine (**29**). Yield: 15%; ^{1}H NMR (400 MHz, $CDCl_3$): δ 1.98-2.04 (m, 2H, CH_2), 2.18 (s, 3H, CH_3), 2.34 (s, 3H, CH_3), 3.10-3.13 (t, *J* = 13.678 Hz, 2H, CH_2), 3.94-3.97 (t, *J* = 13.640 Hz, 2H, CH_2), 6.46 (s, 1H, ArH), 6.61-6.63 (d, *J* = 7.442 Hz, 2H, ArH), 6.95-6.97 (d, *J* = 7.555 Hz, 1H, ArH), 7.11-7.15 (t, *J* = 17.322 Hz, 3H, ArH), 7.26 (s, solv), 7.31-7.35 (m, 2H, ArH). ^{13}C NMR (100 MHz, $CDCl_3$): δ 12.80, 21.64, 30.43, 40.80, 45.24, 111.42, 115.79, 115.96, 118.49, 118.57, 124.44, 130.31, 131.00, 131.07, 135.14, 137.47, 138.85, 144.39, 161.09, 163.06. HRMS (EI): calcd for $C_{20}H_{22}FN_3$, 323.1798; found, $C_{20}H_{23}FN_3$, 324.1870 $[M+H]^+$.

4'-Fluoro-6-methyl-N-(3-(4-methyl-1H-imidazol-1-yl)propyl)-[1,1'-biphenyl]-2-amine (**30**). Yield: 15%; ^{1}H NMR (400 MHz, $CDCl_3$): δ 1.95-2.02 (m, 2H, CH_2), 2.19 (s, 3H, CH_3), 2.27 (s, 3H, CH_3), 3.07-3.10 (t, *J* = 13.755 Hz, 2H, CH_2), 3.90-3.94 (t, *J* = 13.556 Hz, 2H, CH_2), 6.56-6.58 (d, *J* = 7.982 Hz, 2H, ArH), 6.90 (s, 1H, ArH), 7.04-7.16 (m, 4H, ArH), 7.26 (s, solv), 7.33-7.37 (m, 2H, ArH). ^{13}C NMR (100 MHz, $CDCl_3$): δ 12.87, 20.70, 30.21, 40.54, 43.32, 107.80, 116.30, 116.51, 118.90, 119.24, 126.59, 127.28, 128.49, 131.77, 131.85, 133.65, 136.98, 145.15, 160.95, 166.28. HRMS (EI): calcd for $C_{20}H_{22}FN_3$, 323.1798; found, $C_{20}H_{23}FN_3$, 324.1865 $[M+H]^+$.

4',6-Difluoro-N-(3-(4-methyl-1H-imidazol-1-yl)propyl)-[1,1'-biphenyl]-2-amine (**31**). Yield: 20%; ^{1}H NMR (400 MHz, $CDCl_3$): δ 1.94-2.00 (m, 2H, CH_2), 2.20 (s, 3H, CH_3), 3.08-3.11 (t, *J* = 14.105 Hz, 2H, CH_2), 3.60 (s, 1H, NH), 3.88-3.91 (t, *J* = 13.410 Hz, 2H, CH_2), 6.40-6.41 (d, *J* = 8.202 Hz, 1H,

ArH), 6.51-6.56 (m, 2H, ArH), 6.79 (s, 1H, ArH), 7.16-7.20 (m, 3H, ArH), 7.27 (s, solv), 7.29-7.32 (m, 2H, ArH). ^{13}C NMR (100 MHz, $CDCl_3$): δ 12.66, 30.07, 40.70, 43.53, 104.52, 104.70, 105.86, 116.17, 116.34, 118.94, 127.84, 129.66, 129.75, 132.17, 132.24, 146.59, 159.47, 161.54, 163.51. HRMS (EI): calcd for $C_{19}H_{19}F_2N_3$, 327.1547; found, $C_{19}H_{20}F_2N_3$, 328.1622 $[M+H]^+$.

3'-Fluoro-N-(3-(4-methyl-1H-imidazol-1-yl)propyl)-[1,1'-biphenyl]-2-amine (**32**). Yield: 22%; ^{1}H NMR (400 MHz, $CDCl_3$): δ 1.93-2.02 (m, 2H, CH_2), 2.31 (s, 3H, CH_3), 3.10-3.14 (t, *J* = 12.914 Hz, 2H, CH_2), 3.80 (s, 1H, NH), 3.87-3.92 (t, *J* = 14.199 Hz, 2H, CH_2), 6.63-6.66 (d, *J* = 7.987 Hz, 1H, ArH), 6.77-6.78 (t, *J* = 3.616 Hz, 1H, ArH), 6.80-6.82 (d, *J* = 7.992 Hz, 1H, ArH), 6.90 (s, 1H, ArH), 7.04-7.10 (m, 2H, ArH), 7.13-7.19 (m, 2H, ArH), 7.22-7.25 (m, 1H, ArH), 7.26 (s, solv), 7.38-7.45 (m, 1H, ArH). ^{13}C NMR (100 MHz, $CDCl_3$): δ 13.56, 30.47, 40.73, 44.35, 110.55, 115.31, 115.75, 115.96, 117.44, 126.68, 128.91, 130.35, 130.94, 136.11, 136.58, 138.36, 144.64, 160.84, 163.29. HRMS (EI): calcd for $C_{19}H_{20}FN_3$, 309.1641; found, $C_{19}H_{21}FN_3$, 310.1714 $[M+H]^+$.

N-(2-(1H-Imidazol-1-yl)ethyl)-3',4'-dimethoxy-[1,1'-biphenyl]-2-amine (**33**). Yield: 17%; ^{1}H NMR (400 MHz, $CDCl_3$): δ 3.5 (m, 2H, CH_2), 3.84 (s, 3H, OCH_3), 3.91 (s, 3H, OCH_3), 4.05 (s, 1H, NH), 4.11-4.14 (m, 2H, CH_2), 6.66-6.68 (d, *J* = 7.953 Hz, 1H, ArH), 6.79-6.81 (m, 3H, ArH), 6.84 (s, 1H, ArH), 6.89-6.91 (d, *J* = 8.444 Hz, 1H, ArH), 7.02 (s, 1H, ArH), 7.10-7.12 (d, *J* = 7.953 Hz, 1H, ArH), 7.23-7.25 (d, *J* = 8.12 Hz, 1H, ArH), 7.26 (s, solv), 7.40 (s, 1H, ArH). ^{13}C NMR (100 MHz, $CDCl_3$): δ 44.55, 45.69, 55.98, 109.91, 111.58, 112.37, 117.78, 118.89, 121.23, 128.63, 129.68, 130.60, 131.26, 137.23, 143.71, 148.35, 149.23. HRMS (EI): calcd for $C_{19}H_{21}N_3O_2$, 323.1634; found, $C_{19}H_{22}N_3O_2$, 324.1705 $[M+H]^+$.

3',4'-Dimethoxy-N-(2-(2-methyl-1H-imidazol-1-yl)ethyl)-[1,1'-biphenyl]-2-amine (**34**). Yield: 14%; ^{1}H NMR (400 MHz, $CDCl_3$): δ 2.28 (s, 3H, CH_3), 3.45-3.48 (m, 2H, CH_2), 3.83 (s, 3H, OCH_3), 3.91 (s, 3H, OCH_3), 4.01-4.04 (m, 2H, CH_2), 6.65-6.67 (d, *J* = 8.218 Hz, 1H, ArH), 6.74 (s, 1H, ArH), 6.76-6.79 (m, 2H, ArH), 6.81-6.83 (d, *J* = 1.424 Hz, 1H, ArH), 6.88-6.92 (m, 2H, ArH), 7.10-7.12 (dd, *J*= 6.504 Hz, 1H, ArH), 7.23-7.25 (m, 1H, ArH), 7.27 (s, solv). ^{13}C NMR (100 MHz, $CDCl_3$): δ 12.62,

43.95, 53.50, 55.98, 109.83, 111.65, 112.39, 117.83, 119.19, 121.29, 126.65, 128.16, 128.64, 129.90, 130.62, 131.22, 143.74, 148.38, 149.24. HRMS (EI): calcd for $C_{20}H_{23}N_3O_2$, 337.1790; found, $C_{20}H_{24}N_3O_2$, 338.1867 $[M+H]^+$.

3',4'-Dimethoxy-N-(2-(4-methyl-1H-imidazol-1-yl)ethyl)-[1,1'-biphenyl]-2-amine (**35**). Yield: 14%; ^{1}H NMR (400 MHz, $CDCl_3$): δ 2.28 (s, 3H, CH_3), 3.45-3.48 (m, 2H, CH_2), 3.83 (s, 3H, OCH_3), 3.91 (s, 3H, OCH_3), 4.01-4.04 (m, 2H, CH_2), 6.65-6.67 (d, *J* = 8.128 Hz, 1H, ArH), 6.74 (s, 1H, ArH), 6.79 (s, 1H, ArH), 6.81-6.82 (d, *J* = 6.750 Hz, 1H, ArH), 6.88 (s, 1H, ArH), 6.90 (s, 1H, ArH), 6.92 (s, 1H, ArH), 7.10-7.12 (dd, *J* = 9.043 Hz, 1H, ArH), 7.25 (s, 1H, ArH), 7.27 (s, solv). ^{13}C NMR (100 MHz, $CDCl_3$): δ 12.57, 43.96, 44.76, 55.97, 109.83, 111.62, 112.37, 117.84, 119.22, 121.26, 126.28, 128.16, 128.63, 128.83, 130.61, 131.20, 143.71, 148.36, 149.22. HRMS (EI): calcd for $C_{20}H_{23}N_3O_2$, 337.1790; found, $C_{20}H_{24}N_3O_2$, 338.1862 $[M+H]^+$.

N-(2-(1H-Imidazol-1-yl)ethyl)-4'-fluoro-[1,1'-biphenyl]-2-amine (**36**). Yield: 16%; ^{1}H NMR (400 MHz, $CDCl_3$): δ 3.49 (m, 2H, CH_2), 3.93 (s, 1H, NH), 4.03-4.06 (t, *J* = 12.127 Hz, 2H, CH_2), 6.69-6.71 (d, *J* = 8.284 Hz, 1H, ArH), 6.74 (s, 1H, ArH), 6.82-6.86 (t, *J* = 14.763 Hz, 1H, ArH), 6.90 (s, 1H, ArH), 7.02-7.07 (m, 3H, ArH), 7.10-7.12 (d, *J* = 7.815 Hz, 1H, ArH), 7.27-7.29 (t, *J* = 13.907 Hz, 2H, ArH), 7.36-7.42 (m, 1H, ArH). ^{13}C NMR (100 MHz, $CDCl_3$): δ 44.42, 45.69, 110.17, 115.88, 116.10, 117.98, 118.84, 127.31, 128.95, 129.70, 130.67, 130.86, 130.94, 137.21, 143.57, 160.92, 163.38. HRMS (EI): calcd for $C_{17}H_{16}FN_3$, 281.1328; found, $C_{17}H_{17}FN_3$, 282.1404 $[M+H]^+$.

4'-Fluoro-N-(2-(2-methyl-1H-imidazol-1-yl)ethyl)-[1,1'-biphenyl]-2-amine (**37**). Yield: 20%; ^{1}H NMR (400 MHz, $CDCl_3$): δ 2.25 (s, 3H, CH_3), 3.43-3.48 (m, 2H, CH_2), 3.84 (s, 1H, NH), 4.00-4.04 (t, *J* = 11.422 Hz, 2H, CH_2), 6.66-6.70 (m, 2H, ArH), 6.78-6.84 (m, 1H, ArH), 6.87 (d, *J* = 1.324 Hz, 1H, ArH), 7.05-7.06 (m, 1H, ArH), 7.08-7.09 (m, 1H, ArH), 7.12 (s, 1H, ArH), 7.18 (s, 1H, ArH), 7.20-7.21 (d, *J* = 2.336 Hz, 1H, ArH), 7.22-7.24 (t, *J* = 4.583 Hz, 1H, ArH), 7.26 (s, solv). ^{13}C NMR (100 MHz, $CDCl_3$): δ 12.79, 43.88, 44.60, 110.09, 115.87, 116.08, 117.96, 118.98, 127.13, 127.30, 128.95, 130.68, 130.86, 130.94, 134.60, 143.63, 160.92, 163.37. HRMS (EI): calcd for $C_{18}H_{18}FN_3$, 295.1485;

found, $C_{18}H_{19}FN_3$, 296.1557 $[M+H]^+$.

4'-Fluoro-N-(2-(4-methyl-1H-imidazol-1-yl)ethyl)-[1,1'-biphenyl]-2-amine (**38**). Yield: 26%; ^{1}H NMR (400 MHz, $CDCl_3$): δ 2.17 (s, 3H, CH_3), 3.45-3.48 (t, J = 11.899 Hz, 2H, CH_2), 3.84 (s, 1H, NH), 4.03-4.05 (t, J = 10.748 Hz, 2H, CH_2), 6.50 (s, 1H, ArH), 6.65-6.69 (t, J = 15.111 Hz, 1H, ArH), 6.80-6.83 (t, J = 14.753 Hz, 1H, ArH), 7.06-7.12 (m, 5H, ArH), 7.21-7.24 (m, 2H, ArH), 7.26 (s, solv). ^{13}C NMR (100 MHz, $CDCl_3$): δ 12.79, 43.88, 44.60, 110.09, 115.87, 116.08, 117.96, 118.98, 127.13, 127.30, 128.95, 130.68, 130.86, 130.94, 134.60, 143.63, 160.92, 163.37. HRMS (EI): calcd for $C_{18}H_{18}FN_3$, 295.1485; found, $C_{18}H_{19}FN_3$, 296.1554 $[M+H]^+$.

N-(2-(1H-Imidazol-1-yl)ethyl)-3'-fluoro-[1,1'-biphenyl]-2-amine (**39**). Yield: 19%; ^{1}H NMR (400 MHz, $CDCl_3$): δ 3.49 (m, 2H, CH_2), 3.93 (s, 1H, NH), 4.03-4.06 (t, J = 11.939 Hz, 2H, CH_2), 6.69-6.71 (d, J = 7.586 Hz, 1H, ArH), 6.74 (s, 1H, ArH), 6.82-6.86 (t, J = 14.977 Hz, 1H, ArH), 6.90 (s, 1H, ArH), 7.02-7.07 (m, 3H, ArH), 7.10-7.12 (d, J = 8.241 Hz, 1H, ArH), 7.27-7.31 (t, J = 15.197 Hz, 2H, ArH), 7.36-7.42 (m, 1H, ArH). ^{13}C NMR (100 MHz, $CDCl_3$): δ 44.48, 45.76, 110.29, 114.31, 114.51, 116.15, 116.35, 118.01, 118.85, 124.81, 129.21, 129.69, 130.48, 137.13, 143.39, 161.84, 164.30. HRMS (EI): calcd for $C_{17}H_{16}FN_3$, 281.1328; found, $C_{17}H_{17}FN_3$, 282.1403 $[M+H]^+$.

3'-Fluoro-N-(2-(2-methyl-1H-imidazol-1-yl)ethyl)-[1,1'-biphenyl]-2-amine (**40**). Yield: 33%; ^{1}H NMR (400 MHz, $CDCl_3$): δ 2.29 (s, 3H, CH_3), 3.49 (m, 2H, CH_2), 3.93 (s, 1H, NH), 4.03-4.06 (t, J = 11.922 Hz, 2H, CH_2), 6.69-6.71 (d, J = 8.184 Hz, 1H, ArH), 6.74 (s, 1H, ArH), 6.82-6.86 (t, J = 13.919 Hz, 1H, ArH), 6.90 (s, 1H, ArH), 7.07-7.12 (m, 3H, ArH), 7.27-7.31 (t, J = 14.475 Hz, 2H, ArH), 7.36-7.42 (m, 1H, ArH). ^{13}C NMR (100 MHz, $CDCl_3$): δ 12.74, 43.91, 44.70, 110.24, 114.30, 114.51, 116.16, 116.37, 118.02, 118.98, 124.81, 127.21, 129.22, 130.49, 130.65, 143.49, 161.85, 164.31. HRMS (EI): calcd for $C_{18}H_{18}FN_3$, 295.1485; found, $C_{18}H_{19}FN_3$, 296.1556 $[M+H]^+$.

3'-Fluoro-N-(2-(4-methyl-1H-imidazol-1-yl)ethyl)-[1,1'-biphenyl]-2-amine (**41**). Yield: 22%; ^{1}H NMR (400 MHz, $CDCl_3$): δ 2.20 (s, 3H, CH_3), 3.08-3.11 (t, J = 13.145 Hz, 2H, CH_2), 3.90-3.93 (t, J = 12.877 Hz, 2H, CH_2), 6.57 (s, 1H, ArH), 6.64-6.65 (d, J = 8.145 Hz, 1H, ArH), 6.76-6.81 (m, 1H,

ArH), 7.05-7.09 (m, 2H, ArH), 7.11-7.13 (d, J = 7.869 Hz, 1H, ArH), 7.17-7.19 (d, J = 8.091 Hz, 1H, ArH), 7.23-7.25 (d, J = 7.695 Hz, 1H, ArH), 7.26 (s, solv), 7.31 (s, 1H, ArH), 7.39-7.44 (m, 1H, ArH). ^{13}C NMR (100 MHz, $CDCl_3$): δ 12.79, 43.88, 44.60, 110.09, 115.87, 116.08, 117.96, 118.98, 127.13, 127.30, 128.95, 130.68, 130.86, 130.94, 134.60, 143.63, 160.92, 163.37. HRMS (EI): calcd for $C_{18}H_{18}FN_3$, 295.1485; found, $C_{18}H_{19}FN_3$, 296.1556 $[M+H]^+$.

Design and *in silico* analysis

A molecular operating environment (MOE, 2011.10, Chemical Computing Group, Canada) was used. The protein preparation steps involved 3D protonation, energy minimization, and active site identification. The docking template structure of hQC was derived from the crystal structure of hQC bound to the inhibitor **1** (PDB: 3PBB), in which **1** was extracted from the crystal structure of the complex, and all crystal waters were removed. Protein was energy minimized and 3D protonated using the structure preparation module of MOE. Ligand files for the molecular docking studies were prepared in MOE and were followed by energy optimization at a standard MMFF94 force field level, with a 0.0001 kcal/mol energy gradient convergence criterion. The optimized geometries were saved in a molecular data base file for further studies.

The optimized ligands were flexibly docked with the rigid hQC using the MOE-Dock program. Thirty independent docking runs were performed using the MOE docking simulation program. The docked poses were analyzed and the best scored pose for each compound was chosen for further analysis. The illustrated structures were made by PyMOL (Delano Scientific LLC, USA).

The ADMET_BBB and ADMET_AlogP98 of selected compounds were predicted by Discovery Studio (Accelrys Co., Ltd., USA).

Inhibitive activities *in vitro*

Preparation of hQC. Cloning, expression and large scale preparation of hQC were performed according to previous reports.[32-34] The gene for hQC was inserted via the *BamH*I and *Xho*I restriction sites into *Escherichia coli* expression vector pET32a with additional introduction of an N-terminal

His6-tag (primer pair Cs/Cas). Primers, 5-3: ACCT*GGATCC*GCTTCTGCTTGGCCGG, BamHI; 5-3: TATC*CTCGAG*TTACAGGTGCAGGTATTC, XhoI (Takara, China). *E.coli* strain DH5α was used for all cloning procedures. The cDNA was verified by sequencing (Samgon, China). Plasmid DNA was amplified, purified, and linearized. hQC was heterologously expressed in *E.coli* BL21(DE3) using Fernbach flasks at room temperature overnight, and expression induced by addition of 0.2 mM IPTG (isopropyl β-D-1-thiogalactopyranoside). Cells were disrupted with 1 mg/mL lysozyme and a freeze-thaw cycle. The purification of hQC protein followed two chromatographic steps: Ni^{2+}-IMAC (immobilized metal affinity chromatography), and molecular sieve chromatography. QC-containing fractions were pooled and purity was analyzed by SDS-PAGE (15%, sodium dodecyl sulfate polyacrylamide gel electrophoresis) and Coomassie blue staining. The purified hQC enzyme was stored at -80 °C without glycerol.

hQC and inhibitive activities studies. The hQC activity was assayed as described elsewhere.[35] Briefly, for spectrophotometric assessment, the assay reactions (200 μL) consisted of varying concentrations (0-4 mM) of freshly prepared H-gln-gln-H, 30 units/ml glutamic acid dehydrogenase, 0.5 mM $NADH/H^+$, and 15mM α-ketoglutaric acid in 0.05 M Tris-HCl, pH 8.0. Reactions were started by the addition of hQC. Activity was monitored by recording the decrease in absorbance at 340 nm for 15 min.

For the inhibitor testing, the assay reaction composition was the same as described above, except for the addition of different concentrations of the synthesized DPCIs and **1**. The percentage of inhibition at 100 mM was calculated according to the formula: % inhibition = $(V_C - V_S)/V_C$, where V_C is the reaction velocity of control, and V_S is the reaction velocity of samples. All experiments were performed in triplicate. The IC_{50} values were determined graphically from log concentration vs. % inhibition curves.

BBB permeation assay

PAMPA-BBB assay *in vitro* was carried out according to previous reports.[27-29] Simply, test compounds were dissolved in DMSO (2 mg/mL) and the stock solutions were diluted in PBS at pH 8.0

to make secondary stock solutions (100 μg/mL, 5% DMSO). The Millipore MultiScreen® assay system (Millipore, Bedford, MA) was used for the artificial membrane support and as the receiver plate. After the required pretreatment, the filter membrane (hydrophobic PVDF) on the 96-well filtration plate was coated with 6 μL PBL solution in dodecane (20 mg/mL) in each well. The donor well was filled with 250 μL of the secondary stock solution. Then the donor plate was securely placed on the top of an acceptor plate which was pre-filled with equal volumes of blank receiving solution to form a 'sandwich'. After 4 h at 25 °C, the absorbance of solutions in the accepter wells was determined by a multi-wavelength UV plate reader at 290-310 nm. Pe was calculated according to the formula: $Pe = -V_dV_a/[(V_d + V_a)St]\ln(1-A_a/A_e)$, where V_d and V_a are the mean volumes of the donor and accepter solutions, S means the surface area of the artificial membrane, t the incubation time, A_a and A_e the UV absorbance of the accepter well and the theoretical equilibrium absorbance, respectively. Each test compound was analyzed in three wells, and at least in three runs, and the results are given as the mean of the whole data set ± standard deviation.

Inhibitory activities in cells

Vector, cell culture and transfect. The APP695-A673V and the PCMV3-QPCT (human glutaminyl cyclase) plasmids were constructed. Human embryonal kidney cells HEK293T were purchased from the Shanghai Cell Bank (Shanghai, China) and cultured in a humidified atmosphere of 5% CO_2 at 37 °C. According to the manufacturer's manual, HEK293T cells were transfected with the APP695-A673V and PCMV3-QPCT plasmids using Lipofectamin2000 (Invitrogen, USA). Transiently transfected cells were grown with serum-free Opti-MEM for 6 h and afterwards incubated overnight under normal DMEM conditions. Then, transfected HEK293T cells were cultured either in the presence of **28** at a concentration of 10 μM for 0, 6, 12, 24 and 48 h or in concentrations of 0, 1, 10, 50 and 100 μM for 24 h. After the culture, cells and culture media were immediately collected for assay.

QC activities assay. Cells were lysed using tissue grinding tube on ice. The hQC activities in the supernatants were determined using the same method mentioned in *hQC and inhibitive activities*

studies.

pE-Aβ$_{3-42}$ concentrations assay. pE-Aβ$_{3-42}$ concentrations in the cell lysate supernatants and culture media were determined using amyloid-beta (N3pE-42) ELISA kit. Briefly, 100 μl of the sample or 100μl of standard were added to 96-well microtiter-plates coated with anti-human Aβ$_{38-42}$ rabbit IgG affinity purify followed by incubation over night at 4 °C. The next day, plates were washed and incubated with horseradish peroxidase-conjugated antibodies for detecting pE-Aβ$_{3-42}$. After a final washing step, bound enzyme activity was measured using a TMB peroxidase substrate in a colorimetric reaction. The absorbance at 450 nm was determined using a Sunrise plate reader (Tecan, Switzerland).

The anti-AD effects *in vivo*

Animals. All animal experiments were approved by the Animal Ethic Committee at Shenzhen University and were carried out in accordance with the approved guidelines. The B6C3-Tg (APPswe/PSEN1dE9) double-transgenic mice (12 weeks, female) were selected and purchased from Guangdong Medical Laboratory Animal Center (GDMLAC) (Foshan, China), and housed at a 12-h day/12-h night cycle with free access to water and food pellets. Animals were treated with contrast solution (control, C), 2 mg (low dose, L) or 10 mg compound **28** per kg weight (high dose, H) by intraperitoneal injection for 8 weeks respectively.

Behavioral testing. Nesting behavior was used to measure changes in social behavior. Here, the nest-building task was administered with slight modifications as previously reported.[30, 31] At the end of the treatment period, mice were individually housed. Eight pieces of cotton paper were introduced inside the home cage to allow nesting behavior and 24h later the quality of the nest was determined.

QC activities, pE-Aβ$_{3-42}$ and soluble Aβs concentrations assay. One day after the behavioral testing, mice were sacrificed by CO_2 inhalation, the brains were removed, flushed with cold saline and placed on filter paper. Separated hippocampus, cortex and one half-brain were homogenized in PBS (pH 7.6) containing a protease inhibitor cocktail using tissue grinding tube on ice respectively. After centrifugation, these supernatants were used for the followed assay or stored at -80 °C. QC activities

were determined using SensoLyte® green glutaminyl cyclase activity assay kit and the spectrophotometric method mentioned in *hQC and inhibitive activities studies* respectively. pE-Aβ_{3-42} and total soluble Aβs concentrations in these supernatants were determined by amyloid-beta (N3pE-42) ELISA kit and ELISA assay using monoclonal anti-β-amyloid protein (mouse IgG1 isotype) as the first antibody, respectively.

pE-Aβ$_{3-42}$ and total Aβs plaques assay. Mice were anaesthetized with pentobarbital and sequentially perfused transcardially with PBS (pH 7.4) and 4% paraformaldehyde in PBS. The brains were removed and placed in the same 4% paraformaldehyde solution for 24 h at 4 °C, followed by sequential immersion in 10 %, 20 % and 30 % sucrose at 4 °C, at the end of which they had sunk to the bottom of the container. When embedded in OCT, frozen 8 μm sections were prepared with a freezing microtome at -20 - -30 °C, and used for the immunohistochemical analysis. Briefly, after antigen-retrieval (5 min), sections were stained with monoclonal mouse antibody against Aβ-pE3 and monoclonal anti-β-amyloid protein (mouse IgG1 isotype) as first antibody for the detection of pE-Aβ_{3-42} and total Aβs plaques, respectively, over night at 4 °C. Primary antibodies were visualized with secondary horseradish peroxidase-conjugated antibodies and the diaminobenzidine reaction in the presence of H_2O_2. Brain sections were washed extensively, mounted on slides and cover slipped. Plaques were observed and photographed under white light or fluorescent microscopy (CX51, Olympus Corporation, Japan). The photographs were further analyzed by Image-Pro Plus 6.0 and Graphpad Prism 5.

Statistical analysis

The results were expressed as the mean ± SD, or mean of means ± SE. The data of the studies *in vivo* were also evaluated by one-way analysis of variance (ANOVA) followed by a post hoc test, or *t*-test. $p < 0.05$ was considered to be significant.

Supporting Information

Evaluation of the house building capacity of the AD mice by Nesting test and the predicted

ADMET_BBB and ADMET_AlogP98 of selected analogues.

Corresponding Author Information

* Phone: +86 755 8617 2799; E-mail: wuhq@szu.edu.cn.

Notes

The authors declare no competing financial interest.

Author Contributions

Manman Li and Yao Dong contributed equally to this work.

Acknowledgements

This work was supported by the grants of National Natural Science Foundation of China (No. 81573288) and the Science and Technology Planning Project of Guangdong Province (No. 2013B021100022).

Abbreviations used

AD, Alzheimer's disease; QC, glutaminyl cyclase; hQC, human glutaminyl cyclase; DPCI, aiphenyl conjugated imidazole derivatives; BBB, blood brain barrier; PDB, protein data bank; Aβ, β-amyloid; pE-Aβ, pyroglutamate-modified β-amyloid; APP, amyloid precursor protein; SAR, structure-activity relationship; PBL, polar brain lipid; CNS, central nervous system; PAMPA-BBB, parallel artificial membrane permeation assay; ADMET, adsorption distribution metabolism excretion and toxicity; TLC, thin-layer chromatography; MOE, molecular operating environment; IPTG, isopropyl β-D-1-thiogalactopyranoside; IMAC, immobilized metal affinity chromatography; SDS-PAGE, sodium dodecyl sulfate polyacrylamide gel electrophoresis; TMB, 3,3′,5,5′-tetramethylbenzidine; HRP, horseradish peroxidase.

References

1. Dobson, C. M. Alzheimer's disease: addressing a twenty-first century plague. *Rend. Fis. Accad. Lincei* **2015**, *26*, 251-262.

2. Snyder, H. M.; Hendrix, J.; Bain, L. J.; Carrillo, M. C. Alzheimer's disease research in the context of the national plan to address Alzheimer's disease. *Mol. Aspects Med.* **2015**, *43-44*, 16-24.

3. Eisele, Y. S.; Monteiro, C.; Fearns, C.; Encalada, S. E.; Wiseman, R. L.; Powers, E. T.; Kelly, J. W. Targeting protein aggregation for the treatment of degenerative diseases. *Nat. Rev. Drug Discovery* **2015**, *14*, 759-780.

4. Hamley, I. W. The amyloid beta peptide: a chemist's perspective. Role in Alzheimer's and fibrillization. *Chem. Rev.* **2012**, *112*, 5147-5192.

5. LaFerla, F. M.; Green, K. N.; Oddo, S. Intracellular amyloid-beta in Alzheimer's disease. *Nat. Rev. Neurosci.* **2007**, *8*, 499-509.

6. Demetrius, L. A.; Driver, J. A. Preventing Alzheimer's disease by means of natural selection. *J. R. Soc. Interface* **2014**, *12*, 20140919.

7. Bayer, T. A.; Wirths, O. Focusing the amyloid cascade hypothesis on N-truncated Abeta peptides as drug targets against Alzheimer's disease. *Acta Neuropathol.* **2014**, *127*, 787-801.

8. Mehta, D. C.; Short, J. L.; Hilmer, S. N.; Nicolazzo, J. A. Drug access to the central nervous system in Alzheimer's disease: preclinical and clinical insights. *Pharm. Res.* **2015**, *32*, 819-839.

9. Saido, T. C.; Iwatsubo, T.; Mann, D. M.; Shimada, H.; Ihara, Y.; Kawashima, S. Dominant and differential deposition of distinct beta-amyloid peptide species, A beta N3(pE), in senile plaques. *Neuron* **1995**, *14*, 457-466.

10. Wirths, O.; Hillmann, A.; Pradier, L.; Hartig, W.; Bayer, T. A. Oligomeric pyroglutamate amyloid-beta is present in microglia and a subfraction of vessels in patients with Alzheimer's disease: implications for immunotherapy. *J. Alzheimer's Dis.* **2013**, *35*, 741-749.

11. Gunn, A. P.; Masters, C. L.; Cherny, R. A. Pyroglutamate-Abeta: role in the natural history of Alzheimer's disease. *Int. J. Biochem. Cell Biol.* **2010**, *42*, 1915-1918.

12. Schlenzig, D.; Manhart, S.; Cinar, Y.; Kleinschmidt, M.; Hause, G.; Willbold, D.; Funke, S. A.; Schilling, S.; Demuth, H. U. Pyroglutamate formation influences solubility and amyloidogenicity of

amyloid peptides. *Biochemistry* **2009**, *48*, 7072-7078.

13. Nussbaum, J. M.; Schilling, S.; Cynis, H.; Silva, A.; Swanson, E.; Wangsanut, T.; Tayler, K.; Wiltgen, B.; Hatami, A.; Ronicke, R.; Reymann, K.; Hutter-Paier, B.; Alexandru, A.; Jagla, W.; Graubner, S.; Glabe, C. G.; Demuth, H. U.; Bloom, G. S. Prion-like behaviour and tau-dependent cytotoxicity of pyroglutamylated amyloid-beta. *Nature* **2012**, *485*, 651-655.

14. Schilling, S.; Hoffmann, T.; Manhart, S.; Hoffmann, M.; Demuth, H. U. Glutaminyl cyclases unfold glutamyl cyclase activity under mild acid conditions. *FEBS Lett.* **2004**, *563*, 191-196.

15. Schilling, S.; Manhart, S.; Hoffmann, T.; Ludwig, H. H.; Wasternack, C.; Demuth, H. U. Substrate specificity of glutaminyl cyclases from plants and animals. *Biol. Chem.* **2003**, *384*, 1583-1592.

16. Huang, K. F.; Wang, Y. R.; Chang, E. C.; Chou, T. L.; Wang, A. H. A conserved hydrogen-bond network in the catalytic centre of animal glutaminyl cyclases is critical for catalysis. *Biochem. J.* **2008**, *411*, 181-190.

17. Valenti, M. T.; Bolognin, S.; Zanatta, C.; Donatelli, L.; Innamorati, G.; Pampanin, M.; Zanusso, G.; Zatta, P.; Carbonare, L. D. Increased glutaminyl cyclase expression in peripheral blood of Alzheimer's disease patients. *J. Alzheimer's Dis.* **2013**, *34*, 263-271.

18. Schilling, S.; Zeitschel, U.; Hoffmann, T.; Heiser, U.; Francke, M.; Kehlen, A.; Holzer, M.; Hutter-Paier, B.; Prokesch, M.; Windisch, M.; Jagla, W.; Schlenzig, D.; Lindner, C.; Rudolph, T.; Reuter, G.; Cynis, H.; Montag, D.; Demuth, H. U.; Rossner, S. Glutaminyl cyclase inhibition attenuates pyroglutamate Abeta and Alzheimer's disease-like pathology. *Nat. Med.* **2008**, *14*, 1106-1111.

19. Schilling, S.; Appl, T.; Hoffmann, T.; Cynis, H.; Schulz, K.; Jagla, W.; Friedrich, D.; Wermann, M.; Buchholz, M.; Heiser, U.; von Horsten, S.; Demuth, H. U. Inhibition of glutaminyl cyclase prevents pGlu-Abeta formation after intracortical/hippocampal microinjection in vivo/in situ. *J. Neurochem.* **2008**, *106*, 1225-1236.

20. Hennekens, C. H.; B, A. B.; Zivin, R.; Gaziano, J. M. Hypothesis: glutaminyl cyclase inhibitors decrease risks of Alzheimer's disease and related dementias. *Expert Rev. Neurother.* **2015**, *15*, 1245-

1248.

21. Buchholz, M.; Heiser, U.; Schilling, S.; Niestroj, A. J.; Zunkel, K.; Demuth, H. U. The first potent inhibitors for human glutaminyl cyclase: synthesis and structure-activity relationship. *J. Med. Chem.* **2006**, *49*, 664-677.

22. Buchholz, M.; Hamann, A.; Aust, S.; Brandt, W.; Bohme, L.; Hoffmann, T.; Schilling, S.; Demuth, H. U.; Heiser, U. Inhibitors for human glutaminyl cyclase by structure based design and bioisosteric replacement. *J. Med. Chem.* **2009**, *52*, 7069-7080.

23. Ramsbeck, D.; Buchholz, M.; Koch, B.; Bohme, L.; Hoffmann, T.; Demuth, H. U.; Heiser, U. Structure-activity relationships of benzimidazole-based glutaminyl cyclase inhibitors featuring a heteroaryl scaffold. *J. Med. Chem.* **2013**, *56*, 6613-6625.

24. Tran, P. T.; Hoang, V. H.; Thorat, S. A.; Kim, S. E.; Ann, J.; Chang, Y. J.; Nam, D. W.; Song, H.; Mook-Jung, I.; Lee, J.; Lee, J. Structure-activity relationship of human glutaminyl cyclase inhibitors having an N-(5-methyl-1H-imidazol-1-yl)propyl thiourea template. *Bioorg. Med. Chem.* **2013**, *21*, 3821-3830.

25. Brooks, A. F.; Jackson, I. M.; Shao, X.; Kropog, G. W.; Sherman, P.; Quesada, C. A.; Scott, P. J. Synthesis and evaluation of [11C]PBD150, a radiolabeled glutaminyl cyclase inhibitor for the potential detection of Alzheimer's disease prior to amyloid β aggregation. *MedChemComm* **2015**, *6*, 1065-1068.

26. Huang, K. F.; Liaw, S. S.; Huang, W. L.; Chia, C. Y.; Lo, Y. C.; Chen, Y. L.; Wang, A. H. Structures of human Golgi-resident glutaminyl cyclase and its complexes with inhibitors reveal a large loop movement upon inhibitor binding. *J. Biol. Chem.* **2011**, *286*, 12439-12449.

27. Camps, P.; Formosa, X.; Galdeano, C.; Munoz-Torrero, D.; Ramirez, L.; Gomez, E.; Isambert, N.; Lavilla, R.; Badia, A.; Clos, M. V.; Bartolini, M.; Mancini, F.; Andrisano, V.; Arce, M. P.; Rodriguez-Franco, M. I.; Huertas, O.; Dafni, T.; Luque, F. J. Pyrano[3,2-c]quinoline-6-chlorotacrine hybrids as a novel family of acetylcholinesterase- and beta-amyloid-directed anti-Alzheimer compounds. *J. Med. Chem.* **2009**, *52*, 5365-5379.

28. Di, L.; Kerns, E. H.; Fan, K.; McConnell, O. J.; Carter, G. T. High throughput artificial membrane permeability assay for blood–brain barrier. *Eur. J. Med. Chem.* **2003**, *38*, 223-232.

29. Zhu, C.; Jiang, L.; Chen, T.-M.; Hwang, K.-K. A comparative study of artificial membrane permeability assay for high throughput profiling of drug absorption potential. *Eur. J. Med. Chem.* **2002**, *37*, 399-407.

30. Deacon, R. M.; Cholerton, L. L.; Talbot, K.; Nair-Roberts, R. G.; Sanderson, D. J.; Romberg, C.; Koros, E.; Bornemann, K. D.; Rawlins, J. N. Age-dependent and -independent behavioral deficits in Tg2576 mice. *Behav. Brain Res.* **2008**, *189*, 126-138.

31. Deacon, R. M. Assessing nest building in mice. *Nat. Protoc.* **2006**, *1*, 1117-1119.

32. Koch, B.; Buchholz, M.; Wermann, M.; Heiser, U.; Schilling, S.; Demuth, H. U. Probing secondary glutaminyl cyclase (QC) inhibitor interactions applying an in silico-modeling/site-directed mutagenesis approach: implications for drug development. *Chem. Biol. Drug Des.* **2012**, *80*, 937-946.

33. Schilling, S.; Hoffmann, T.; Rosche, F.; Manhart, S.; Wasternack, C.; Demuth, H. U. Heterologous expression and characterization of human glutaminyl cyclase: evidence for a disulfide bond with importance for catalytic activity. *Biochemistry* **2002**, *41*, 10849-10857.

34. Ruiz-Carrillo, D.; Koch, B.; Parthier, C.; Wermann, M.; Dambe, T.; Buchholz, M.; Ludwig, H. H.; Heiser, U.; Rahfeld, J. U.; Stubbs, M. T.; Schilling, S.; Demuth, H. U. Structures of glycosylated mammalian glutaminyl cyclases reveal conformational variability near the active center. *Biochemistry* **2011**, *50*, 6280-6288.

35. Schilling, S.; Niestroj, A. J.; Rahfeld, J. U.; Hoffmann, T.; Wermann, M.; Zunkel, K.; Wasternack, C.; Demuth, H. U. Identification of human glutaminyl cyclase as a metalloenzyme. Potent inhibition by imidazole derivatives and heterocyclic chelators. *J. Biol. Chem.* **2003**, *278*, 49773-49779.

Tables

Table 1. The inhibitory activities of imidazole unsubstituted analogues on hQC

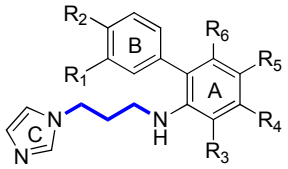

Cpd.	R_1	R_2	R_3	R_4	R_5	R_6	% inhibition at 100 μM *	IC_{50} (μM)
2	OCH_3	OCH_3	H	H	H	H	85.34±2.04	2.08
3	OCH_3	OCH_3	CH_3	H	H	H	51.74±7.69	
4	OCH_3	OCH_3	F	H	H	H	94.67±1.78	1.38
5	OCH_3	OCH_3	H	CH_3	H	H	-**	
6	OCH_3	OCH_3	H	H	$CH(CH_3)_2$	H	51.23±3.8	
7	OCH_3	OCH_3	H	H	H	CH_3	96.14±0.89	0.64
8	H	F	H	H	H	H	85.11±7.03	3.02
9	H	F	H	H	H	CH_3	92.83±2.25	0.83
10	H	F	H	H	H	F	85.50±1.46	1.56
11	F	H	H	H	H	H	78.21±4.67	

* % inhibition at 100 μM means percentage of inhibition at 100 μM; ** - means no obvious activity.

Table 2. The inhibitory activities of analogues with 2'-methyl substituted imidazole ring on hQC

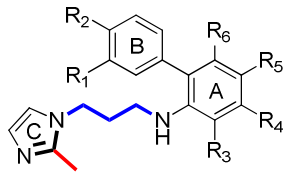

Cpd.	R_1	R_2	R_3	R_4	R_5	R_6	% inhibition at 100 μM
12	OCH_3	OCH_3	CH_3	H	H	H	-
13	OCH_3	OCH_3	H	CH_3	H	H	8.61±3.57
14	OCH_3	OCH_3	H	H	$CH(CH_3)_2$	H	11.83±1
15	H	F	H	H	H	H	37.04±4.38
16	H	F	H	H	H	CH_3	48.05±3.03
17	H	F	H	H	H	F	45.95±24.76
18	H	F	H	CH_3	H	H	41.97±9.76
19	F	H	H	H	H	H	20.41±4.36
20	F	H	H	H	$CH(CH_3)_2$	H	72.48±9.18

Table 3. The inhibitory activities of analogues with 4'-methyl substituted imidazole ring on hQC

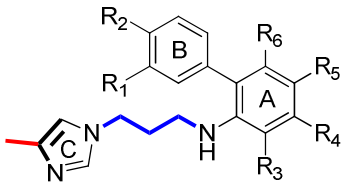

Cpd.	R_1	R_2	R_3	R_4	R_5	R_6	% inhibition at 100 μM	IC_{50} (μM)
21	OCH_3	OCH_3	H	H	H	H	93.61±3.8	0.89
22	OCH_3	OCH_3	CH_3	H	H	H	-	
23	OCH_3	OCH_3	F	H	H	H	95.19±2.63	0.50
24	OCH_3	OCH_3	H	CH_3	H	H	94.48±2.55	2.57
25	OCH_3	OCH_3	H	H	CH_3	H	95.91±1.63	0.94
26	OCH_3	OCH_3	H	H	$CH(CH_3)_2$	H	-	
27	OCH_3	OCH_3	H	H	H	CH_3	96.24±1.54	0.70
28	H	F	H	H	H	H	92.57±3.3	1.23
29	H	F	H	CH_3	H	H	92.41±2.01	1.62
30	H	F	H	H	H	CH_3	94.65±2.00	0.79
31	H	F	H	H	H	F	95.70±2.62	0.88
32	F	H	H	H	H	H	87.28±7.71	15.50

Table 4. The inhibitory activities of analogues with short linker on hQC

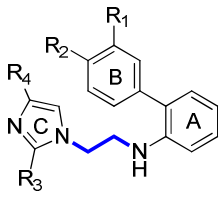

Cpd.	R_1	R_2	R_3	R_4	% inhibition at 100 μM
33	OCH_3	OCH_3	H	H	34.55±4.01
34	OCH_3	OCH_3	CH_3	H	-
35	OCH_3	OCH_3	H	CH_3	7.99±4.64
36	H	F	H	H	-
37	H	F	CH_3	H	-
38	H	F	H	CH_3	8.82±13.96
39	F	H	H	H	39.6±1.19
40	F	H	CH_3	H	8.86±4.81
41	F	H	H	CH_3	19.05±4.85

Scheme 1

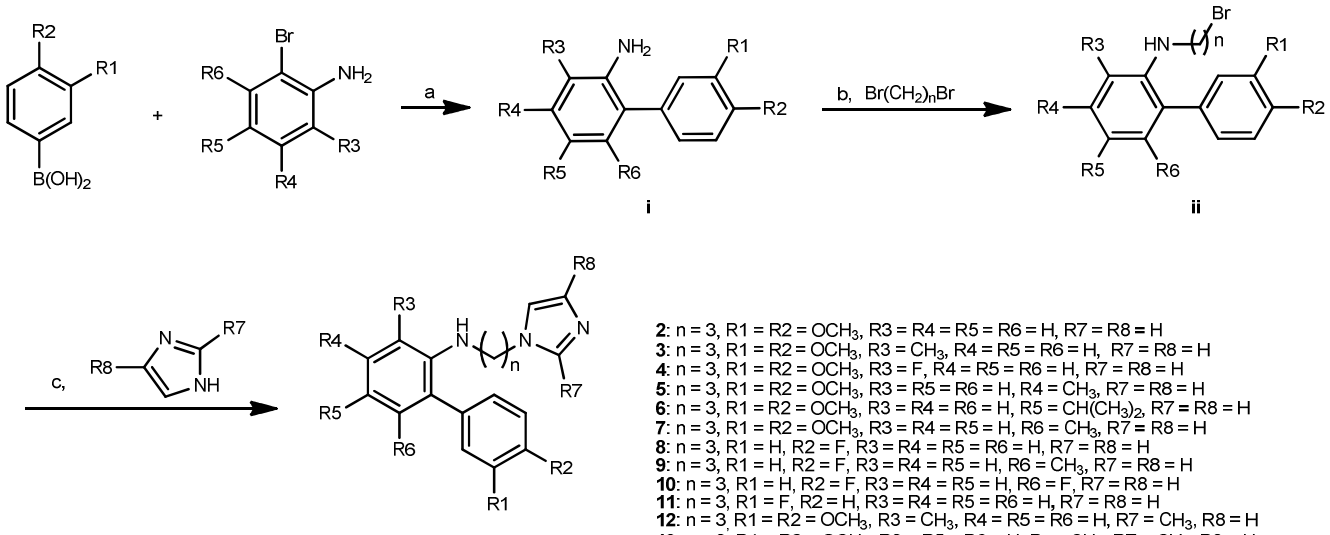

2: n = 3, R1 = R2 = OCH_3, R3 = R4 = R5 = R6 = H, R7 = R8 = H
3: n = 3, R1 = R2 = OCH_3, R3 = CH_3, R4 = R5 = R6 = H, R7 = R8 = H
4: n = 3, R1 = R2 = OCH_3, R3 = F, R4 = R5 = R6 = H, R7 = R8 = H
5: n = 3, R1 = R2 = OCH_3, R3 = R5 = R6 = H, R4 = CH_3, R7 = R8 = H
6: n = 3, R1 = R2 = OCH_3, R3 = R4 = R6 = H, R5 = $CH(CH_3)_2$, R7 = R8 = H
7: n = 3, R1 = R2 = OCH_3, R3 = R4 = R5 = H, R6 = CH_3, R7 = R8 = H
8: n = 3, R1 = H, R2 = F, R3 = R4 = R5 = R6 = H, R7 = R8 = H
9: n = 3, R1 = H, R2 = F, R3 = R4 = R5 = H, R6 = CH_3, R7 = R8 = H
10: n = 3, R1 = H, R2 = F, R3 = R4 = R5 = H, R6 = F, R7 = R8 = H
11: n = 3, R1 = F, R2 = H, R3 = R4 = R5 = R6 = H, R7 = R8 = H
12: n = 3, R1 = R2 = OCH_3, R3 = CH_3, R4 = R5 = R6 = H, R7 = CH_3, R8 = H
13: n = 3, R1 = R2 = OCH_3, R3 = R5 = R6 = H, R_4 = CH_3, R7 = CH_3, R8 = H
14: n = 3, R1 = R2 = OCH_3, R3 = R4 = R6 = H, R5 = $CH(CH_3)_2$, R7 = CH_3, R8 = H
15: n = 3, R1 = H, R2 = F, R3 = R4 = R5 = R6 = H, R7 = CH_3, R8 = H
16: n = 3, R1 = H, R2 = F, R3 = R4 = R5 = H, R6 = CH_3, R7 = CH_3, R8 = H
17: n = 3, R1 = H, R2 = F, R3 = R4 = R5 = H, R6 = F, R7 = CH3, R8 = H
18: n = 3, R1 = H, R2 = F, R3 = R5 = R6 = H, R4 = CH_3, R7 = CH_3, R8 = H
19: n = 3, R1 = F, R2 = H, R3 = R4 = R5 = R6 = H, R7 = CH_3, R8 = H
20: n = 3, R1 = F, R2 = H, R3 = R4 = R6 = H, R5 = $CH(CH_3)_2$, R7 = CH_3, R8 = H
21: n = 3, R1 = R2 = OCH_3, R3 = R4 = R5 = R6 = H, R7 = H, R8 = CH_3
22: n = 3, R1 = R2 = OCH_3, R3 = CH_3, R4 = R5 = R6 = H, R7 = H, R8 = CH_3
23: n = 3, R1 = R2 = OCH_3, R3 = F, R4 = R5 = R6 = H, R7 = H, R8 = CH_3
24: n = 3, R1 = R2 = OCH_3, R3 = R5 = R6 = H, R4 = CH_3, R7 = H, R8 = CH_3
25: n = 3, R1 = R2 = OCH_3, R3 = R4 = R6 = H, R5 = CH_3, R7 = H, R8 = CH_3
26: n = 3, R1 = R2 = OCH_3, R3 = R4 = R6 = H, R5 = $CH(CH_3)_2$, R7 = H, R8 = CH_3
27: n = 3, R1 = R2 = OCH_3, R3 = R4 = R5 = H, R6 = CH_3, R7 = H, R8 = CH_3

28: n = 3, R1 = H, R2 = F, R3 = R4 = R5 = R6 = H, R7 = H, R8 = CH_3
29: n = 3, R1 = H, R2 = F, R3 = R5 = R6 = H, R4 = CH_3, R7 = H, R8 = CH_3
30: n = 3, R1 = H, R2 = F, R3 = R4 = R5 = H, R6 = CH_3, R7 = H, R8 = CH_3
31: n = 3, R1 = H, R2 = F, R3 = R4 = R5 = H, R6 = F, R7 = H, R8 = CH_3
32: n = 3, R1 = F, R2 = H, R3 = R4 = R5 = R6 = H, R7 = H, R8 = CH_3
33: n = 2, R1 = R2 = OCH_3, R3 = R4 = R5 = R6 = H, R7 = R8 = H
34: n = 2, R1 = R2 = OCH_3, R3 = R4 = R5 = R6 = H, R7 = CH_3, R8 = H
35: n = 2, R1 = R2 = OCH_3, R3 = R4 = R5 = R6 = H, R7 = H, R8 = CH_3
36: n = 2, R1 = H, R2 = F, R3 = R4 = R5 = R6 = H, R7 = R8 = H
37: n = 2, R1 = H, R2 = F, R3 = R4 = R5 = R6 = H, R7 = CH_3, R8 = H
38: n = 2, R1 = H, R2 = F, R3 = R4 = R5 = R6 = H, R7 = H, R8 = CH_3
39: n = 2, R1 = F, R2 = H, R3 = R4 = R5 = R6 = H, R7 = R8 = H
40: n = 2, R1 = F, R2 = H, R3 = R4 = R5 = R6 = H, R7 = CH_3, R8 = H
41: n = 2, R1 = F, R2 = H, R3 = R4 = R5 = R6 = H, R7 = H, R8 = CH_3

Reagents and conditions: (a) $Pd(DPPF)_2Cl_2$, K_2CO_3, 1,4-Dioxane, reflux, 3h, 100 °C, Ar; (b) acetonitrile, K_2CO_3, reflux, overnight; (c) acetonitrile, K_2CO_3, reflux, overnight.

Legends

Scheme 1. Reagents and conditions: (a) $Pd(DPPF)_2Cl_2$, K_2CO_3, 1,4-Dioxane, reflux, 3h, 100 °C, Ar; (b) acetonitrile, K_2CO_3, reflux, overnight; (c) acetonitrile, K_2CO_3, reflux, overnight.

Figure 1. The proposed skeleton of DPCIs and the docked model with hQC.

A, the structure of **1** (upper) and prototypical DPCI (**2**, down); B-C, the overlay pose of **1** (green) and **2** (brown) in the catalytic active region of hQC (PDB: 3PBB). Protein surface is illustrated (B). Compound **2** was predicted to interact with hQC in a manner similar to **1**, the important residues were shown using stick format (C).

Figure 2. Docked conformations of DPCIs with hQC.

A, binding mode of **1** with hQC (PDB: 3PBB) in the crystal structure; B-D, docked poses of potent inhibitors **2**, **23** and **28** with hQC respectively; E & F, docked poses of inactive inhibitors **36** and **37** with hQC respectively. The inhibitors are shown in stick mode and hQC is shown in yellow cartoons. Interactions between the protein residues and inhibitors with the catalytic zinc ion at the bottom of the pocket are shown in dash lines.

Figure 3. Permeability of **28** determined by the PAMPA-BBB assay.

Figure 4. Analysis of the inhibitory potency of **28** in transfected HEK293T cells.

A, inhibitory effects of **28** on hQC in PCMV3-QPCT (hQC) and APP695-A673V transfected HEK293T cells which were treated for 6, 12, 24 and 48 h at the concentration of 10 μM; B, inhibitory effects of **28** on hQC in transfected HEK293T cells which were treated for 24 h at the concentrations of 1, 10, 50 and 100μM; C, quantification of the pE-$A\beta_{3\text{-}42}$ in transfected HEK293T cells which were treated with **28** for 24 h at the concentrations of 0, 1, 10, 50 and 100 μM using amyloid-beta (N3pE-42) ELISA kit. All experiments were performed in triplicate. Data are expressed as mean ± SD.

Figure 5. The effects of **28** on the AD pathogenesis in the B6C3-Tg (APPswe/PSEN1dE9) double-transgenic mice.

A, determination of QC activities in hippocampus, cortex and total brain of AD mice treated with **28** at

concentrations of 0 (C), 2 mg (L) and 10 mg per kg weight (H) by intraperitoneal injection for 2 months by SensoLyte® green glutaminyl cyclase activity assay kit; B, determination of QC activities in hippocampus, cortex and total brain of AD mice by GD-QC assay. C, quantification of pE-$A\beta_{3-42}$ in hippocampus, cortex and total brain of AD mice using amyloid-beta (N3pE-42) ELISA kit; D, quantification of total soluble Aβs in the supernatants of hippocampus, cortex and total brain of AD mice using ELISA analysis; E, immunohistochemical detection of pE-$A\beta_{3-42}$ plaques in hippocampus and cortex area in the brain of AD mice; F, quantification of the pE-$A\beta_{3-42}$ plaque load based on the histochemical staining in E; G, immunohistochemical detection of total Aβs plaques in hippocampous and cortex area in the brain of AD mice; H, quantification of the Aβs plaque load based on the histochemical staining in G; I, evaluation of the house building capacity of the AD mice by Nesting test. To reduce the within group variance, only female mice were used in the study (n = 4 per group). Data are expressed as mean ± SE. * means $p < 0.05$ versus control.

Figures

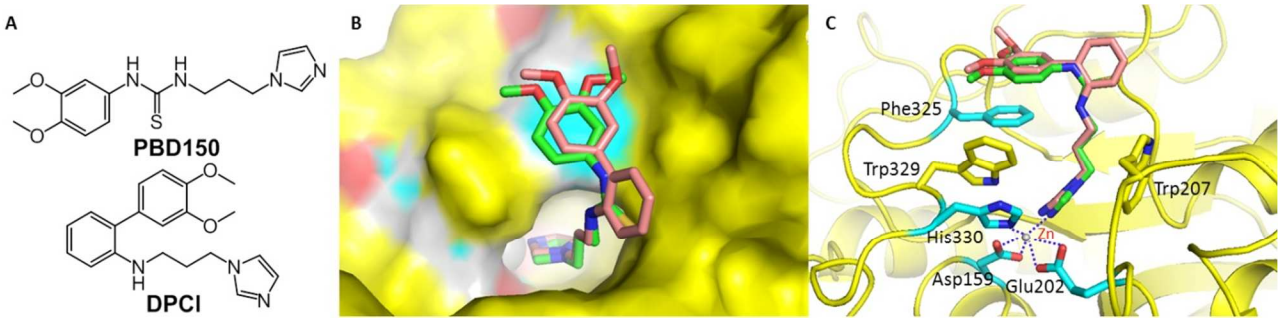

Figure 1. The proposed skeleton of DPCIs and the docked model with hQC.

A, the structure of **1** (upper) and prototypical DPCI (**2**, down); B-C, the overlay pose of **1** (green) and **2** (brown) in the catalytic active region of hQC (PDB: 3PBB). Protein surface is illustrated (B). Compound **2** was predicted to interact with hQC in a manner similar to **1**, the important residues were shown using stick format (C).

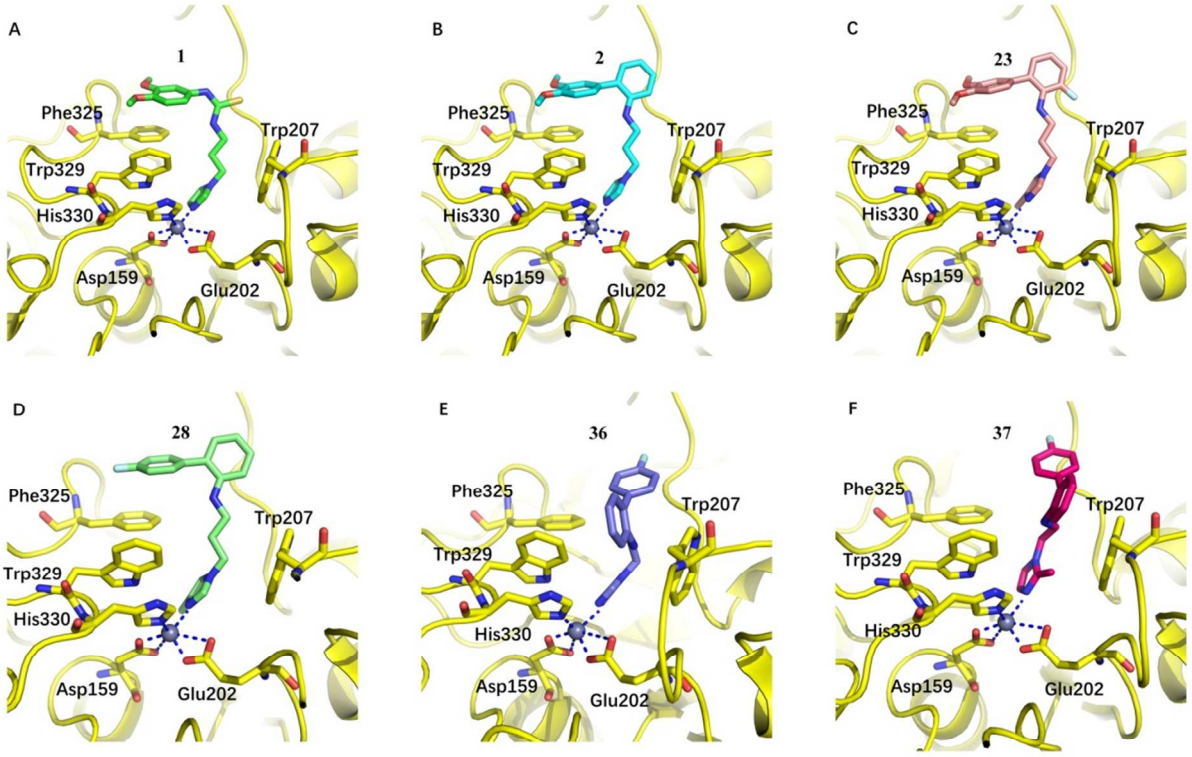

Figure 2. Docked conformations of DPCIs with hQC.

A, binding mode of **1** with hQC (PDB: 3PBB) in the crystal structure; B-D, docked poses of potent inhibitors **2**, **23** and **28** with hQC respectively; E & F, docked poses of inactive inhibitors **36** and **37** with hQC respectively. The inhibitors are shown in stick mode and hQC is shown in yellow cartoons. Interactions between the protein residues and inhibitors with the catalytic zinc ion at the bottom of the pocket are shown in dash lines.

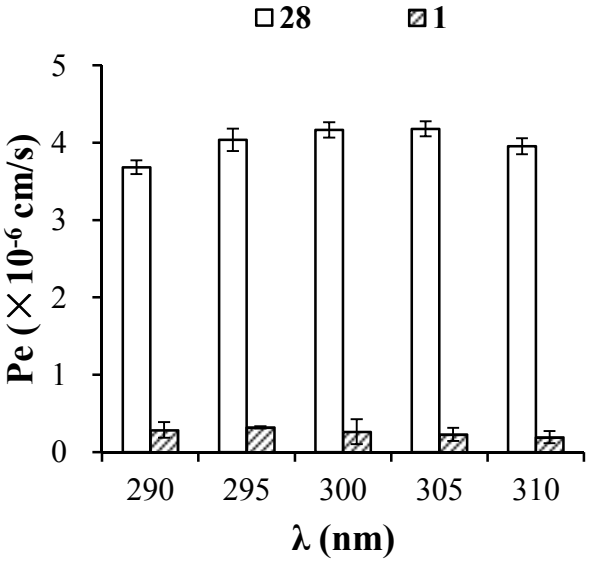

Figure 3. Permeability of **28** determined by the PAMPA-BBB assay.

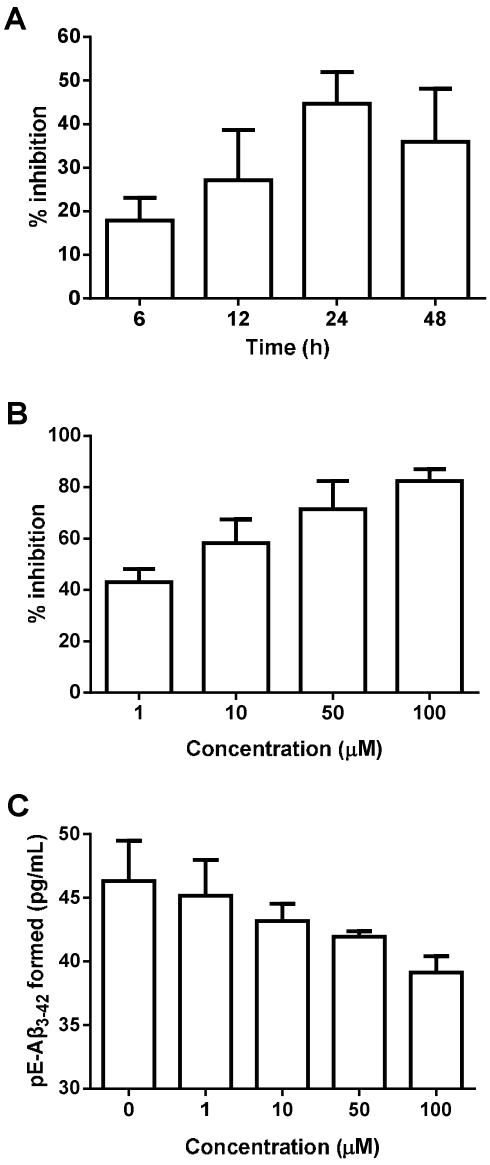

Figure 4. Analysis of the inhibitory potency of **28** in transfected HEK293T cells.

A, inhibitory effects of **28** on hQC in PCMV3-QPCT (hQC) and APP695-A673V transfected HEK293T cells which were treated for 6, 12, 24 and 48 h at the concentration of 10 μM; B, inhibitory effects of **28** on hQC in transfected HEK293T cells which were treated for 24 h at the concentrations of 1, 10, 50 and 100μM; C, quantification of the pE-$A\beta_{3-42}$ in transfected HEK293T cells which were treated with **28** for 24 h at the concentrations of 0, 1, 10, 50 and 100 μM using amyloid-beta (N3pE-42) ELISA kit. All experiments were performed in triplicate. Data are expressed as mean ± SD.

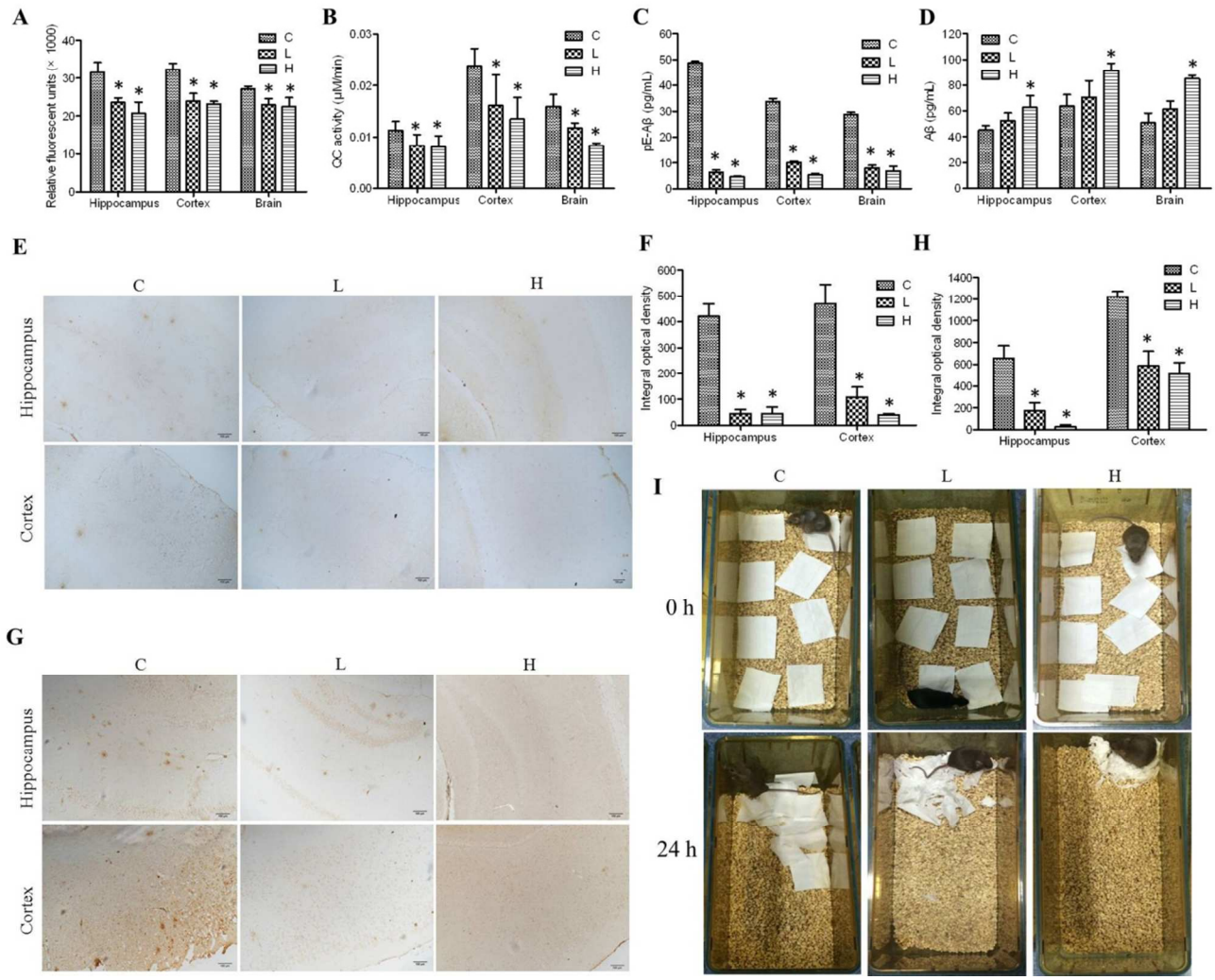

Figure 5. The effects of **28** on the AD pathogenesis in the B6C3-Tg (APPswe/PSEN1dE9) double-transgenic mice.

A, determination of QC activities in hippocampus, cortex and total brain of AD mice treated with **28** at concentrations of 0 (C), 2 mg (L) and 10 mg per kg weight (H) by intraperitoneal injection for 2 months by SensoLyte® green glutaminyl cyclase activity assay kit; B, determination of QC activities in hippocampus, cortex and total brain of AD mice by GD-QC assay. C, quantification of pE-$A\beta_{3\text{-}42}$ in hippocampus, cortex and total brain of AD mice using amyloid-beta (N3pE-42) ELISA kit; D, quantification of total soluble Aβs in the supernatants of hippocampus, cortex and total brain of AD mice using ELISA analysis; E, immunohistochemical detection of pE-$A\beta_{3\text{-}42}$ plaques in hippocampus and cortex area in the brain of AD mice; F, quantification of the pE-$A\beta_{3\text{-}42}$ plaque load based on the

histochemical staining in E; G, immunohistochemical detection of total Aβs plaques in hippocampous and cortex area in the brain of AD mice; H, quantification of the Aβs plaque load based on the histochemical staining in G; I, evaluation of the house building capacity of the AD mice by Nesting test. To reduce the within group variance, only female mice were used in the study (n = 4 per group). Data are expressed as mean ± SE. * means $p < 0.05$ versus control.

Table of Contents graphic